M 2020

U.PORTO
FEUP FACULDADE DE ENGENHARIA
UNIVERSIDADE DO PORTO

THE USE OF MEMBRANE REACTORS IN REACTIONS OF CARBON DIOXIDE HYDROGENATION

IGOR GABRIEL ITO IWAKIRI

DISSERTAÇÃO DE MESTRADO APRESENTADA
À FACULDADE DE ENGENHARIA DA UNIVERSIDADE DO PORTO EM
ENGENHARIA QUÍMICA

Master in Chemical Engineering

The use of membrane reactors in reactions of carbon dioxide hydrogenation

Master Dissertation

of

Igor Gabriel Ito Iwakiri

Developed within the course of Dissertation

held in

Laboratory of Process Engineering, Environment, Biotechnology and Energy

Supervisor at FEUP:

Prof. Dr. Luis Miguel Palma Madeira

Dr. Carlos Eduardo Geraldes de Vasconcelos Miguel

July 2020

Acknowledgment

Foremost, I would like to express my sincere thanks to my advisor Prof. Dr. Luis Miguel Madeira for the opportunity of working in a field of knowledge as interesting and versatile as the chemical reaction engineering, for his attention, instructions, and patience.

My gratitude also goes to Dr. Carlos Miguel, for his availability, corrections, and his great contribution in this work.

I would like to thank PhD Student Catarina Faria for her availability and patience.

I am grateful to my family, for the unconditional support.

I am also grateful to all the professors responsible for my evolution over the past five years, both from the University of Coimbra and the University of Porto.

Thanks to them, I have learned that every system has a set of rules that relate all its variables. I have learned how to relate those variables in an index, and how to optimize it. I believe that, from now on, it is a matter of discovering for myself which indexes are worth optimizing.

This work was financially supported by:

- Base Funding - UIDB/00511/2020 of the Laboratory for Process Engineering, Environment, Biotechnology and Energy – LEPABE - funded by national funds through the FCT/MCTES (PIDDAC);

- Project POCI-01-0145-FEDER-030277, funded by FEDER funds through COMPETE2020 – Programa Operacional Competitividade e Internacionalização (POCI) and by national funds (PIDDAC) through FCT/MCTES.

Abstract

Although fossil fuels have been essential for the exponential technological development of the humanity, their slow replacement and the changes caused in the biosphere by their use mean that an energy matrix sustained by their extraction cannot be used in the long term. In this sense, one of the alternatives is the Power-to-X (PtX) technology, capable of chemically storing electrical energy from renewable sources, such as the sun and the wind, in gaseous or liquid fuels. Currently, PtX is technically limited by two processes: water electrolysis and CO_2 hydrogenation.

To obtain greater conversions in the hydrogenation of CO_2, or similar results in milder conditions of pressure and temperature when compared to those reached in a conventional reactor, reducing the operational costs, it is proposed to use a membrane reactor capable of separating one of the products - water - from the catalytic bed, this way shifting the chemical equilibrium towards greater fuel production - in this work, methane or methanol.

In order to study the influence of intensive variables in a traditional or membrane reactor, a MATLAB program was developed, based on previous works, which is capable of simulating simultaneous gas phase reactions in catalytic non-isothermal tubular reactors with axial dispersion, non constant superficial velocity and pressure drop. Simulations were carried out, in ranges between 250 °C - 410 °C and 1 atm - 7 atm for methane production and 150 °C - 310 °C and 10 atm - 70 atm for methanol production. Since the available hydrophilic SOD membrane permeates both reactants, CO_2 and H_2, at kinetically viable temperatures to the processes, it was considered to feed both the retentate and permeate with such reactants to prevent their loss from the catalytic bed.

For methane, although the catalytic bed (retentate zone) becomes more efficient in converting reactants fed into it, much of the reactants fed in the permeate zone do not enter the catalytic bed. Besides, since the methane produced also permeates the membrane, reactants unable to enter the bed from the permeated side are mixed with such product, making it more difficult to recycle. For methanol, its permeance was not significant in the studied temperature range. Thus, in addition to being able to increase the methanol yield of the catalytic bed by up to 18% due to the shift of chemical equilibrium, the reactants fed in the permeate side that could not enter the catalytic bed leave the system mixed mostly with water vapor (the highest molar fraction of methanol observed in the permeate was 0.005), which facilitates the recycling of such reactants by simple condensation.

Finally, a fictitious membrane, which permeates only water, is simulated for methane and methanol production, being able to decrease the operational temperature for methane production from 410 °C to 360 °C (as compared to a traditional reactor), showing the high potential of membrane reactors to optimize processes such as CO_2 hydrogenation, depending on the progress in materials science.

Keywords (theme): Power-to-X, Membrane Reactors, MATLAB, Methane, Methanol.

Resumo

Apesar de os combustíveis fósseis terem sido essenciais para o exponencial desenvolvimento tecnológico da humanidade, a sua lenta reposição natural e as alterações causadas na biosfera levam a que a matriz energética baseada no seu uso não possa ser utilizada a longo prazo. Surge, assim, como alternativa, a tecnologia Power-to-X (PtX) capaz de armazenar quimicamente a energia elétrica proveniente de fontes renováveis (e.g. Sol e vento) em combustíveis gasosos ou líquidos. Atualmente a PtX é limitada tecnicamente por dois processos: a eletrólise da água e a hidrogenação do CO_2.

Para se obterem maiores conversões na hidrogenação de CO_2 ou resultados semelhantes aos de um reator tradicional em condições de pressão e temperatura mais moderadas, reduzindo-se os custos operatórios, é proposto o uso de um reator de membrana capaz de separar um dos produtos (a água) do leito catalítico a fim de deslocar o equilíbrio para maiores produções do combustível – neste trabalho, metano ou metanol.

Com o objetivo de estudar a influência de variáveis intensivas num reator tradicional ou de membrana, foi desenvolvido, partindo de trabalhos anteriores, um programa em MATLAB capaz de simular reações gasosas simultâneas em reatores tubulares não isotérmicos com dispersão axial, com velocidade variável e queda de pressão no leito. Realizaram-se simulações nas gamas (250-410) ℃ e (1–7) atm para a produção de metano; e nas gamas (150-310) ℃ e (10-70) atm, no caso do metanol. Uma vez que, em condições de temperatura cineticamente viáveis aos processos, a membrana SOD hidrofílica disponível permeia ambos os reagentes, CO_2 e H_2, foi necessário alimentar tanto o retido como o permeado com tais reagentes, de forma a impedir a sua perda através do leito catalítico.

Para o metano, apesar de o leito catalítico (zona do retido) se tornar mais eficiente na conversão dos reagentes que lá passam, boa parte dos reagentes alimentados no permeado não entram no leito. Além disso, uma vez que a membrana também permeia o metano produzido, os reagentes incapazes de entrar no leito são misturados com este produto gasoso, dificultando a sua reciclagem. Para o metanol, a sua permeância à membrana não se mostrou significativa no intervalo de temperatura estudado. Dessa forma, além de ser possível aumentar o rendimento de metanol até 18% devido ao deslocamento de equilíbrio químico, a corrente de reagentes que não entrou no leito catalítico sai do sistema misturada maioritariamente com vapor de água (a maior fração molar de metanol observada no permeado foi de 0.005), o que facilita a reciclagem de tais reagentes por simples condensação.

Finalmente, é considerada na simulação uma membrana fictícia que permeia apenas água, para a produção de metano e metanol, a qual é capaz de reduzir a temperatura da produção de metano de 410 ℃ para 360 ℃ (comparativamente a um reator tradicional), mostrando, assim, o alto potencial dos reatores de membrana em otimizarem processos como a hidrogenação de CO_2, consoante o avanço na ciência de materiais.

Palavras-chave: Power-to-X, Reatores de Membrana, MATLAB, Metano, Metanol.

Declaration

I hereby declare, on my word of honor, that this work is original and that all non-original contributions are indicated and due reference is given to the author and source

Igor Gabriel Ito Iwakiri

06/07/2020

Index

List of Figures

List of Tables

Notation and Glossary

A	Axial Area	m^2
b	Coefficient of Adsorption	bar^{-1}
C	Molar Concentration	$mol \cdot m^{-3}$
C_p	Massic Heat Capacity	$J \cdot K^{-1} \cdot kg^{-1}$
D_{ea}	Massic Axial Dispersion Coefficient	$m^2 \cdot s^{-1}$
d_p	Mean Diameter of a Particle of Catalyst	m
E_a	Apparent Activation Energy for Permeation	$J \cdot mol^{-1}$
F	Molar Flow Rate	$mol \cdot s^{-1}$
H	Enthalpy	$J \cdot mol^{-1}$
J	Molar Flux Through the Membrane	$mol \cdot s^{-1} \cdot m^{-2}$
$K_{2.1}$	Chemical Equilibrium Constant of Reaction 2.1	bar^{-2}
$K_{2.2}$	Chemical Equilibrium Constant of Reaction 2.2	Dimensionless
$K_{2.3}$	Chemical Equilibrium Constant of Reaction 2.3	bar^{-2}
$K_{2.4}$	Chemical Equilibrium Constant of Reaction 2.4	$atm^{-0.304}$
$k_{2.1}$	Kinetic Constant of Reaction 2.1	$mol \cdot s^{-1} \cdot bar^{-1} \cdot kg^{-1}$
$k_{2.2}$	Kinetic Constant of Reaction 2.2	$mol \cdot s^{-1} \cdot bar^{-1} \cdot kg^{-1}$
$k_{2.3}$	Kinetic Constant of Reaction 2.3	$mol \cdot s^{-1} \cdot bar^{-1} \cdot kg^{-1}$
$k_{2.4}$	Kinetic Constant of Reaction 2.4	$mol \cdot s^{-1} \cdot atm^{-0.76} \cdot g^{-1}$
L	Reactor Length	m
P	Total Pressure	bar
p	Partial Pressure	bar
$Perm$	Permeance	$mol \cdot m^{-2} \cdot s^{-1} \cdot Pa^{-1}$
R	Ideal Gas Constant	$J \cdot K^{-1} \cdot mol^{-1}$
r	Radius	m
T	Temperature	K
u_0	Superficial Velocity	$m \cdot s^{-1}$
U	Global Coefficient of Heat Flux	$W \cdot m^{-2} \cdot K^{-1}$
W	Mass of Catalyst	kg
X	Conversion	Dimensionless
z	Dimensionless Reactor Length	Dimensionless
ε	Porosity	Dimensionless
ρ	Density	$kg \cdot m^{-3}$
α	Stoichiometric Coefficient	Dimensionless
$\mathfrak{R}$	Reaction Rate	$mol \cdot s^{-1} \cdot kg^{-1}$
λ_{ea}	Thermal Axial Dispersion Coefficient	$W \cdot m^{-1} \cdot K^{-1}$
μ	Viscosity	$Pa \cdot s$
β	Pre-exponential factor	$mol \cdot m^{-2} \cdot s^{-1} \cdot Pa^{-1}$

Indexes

0	At the first point inside the reactor
∞	At the furnace
b	Regarding the Bulk
f	Regarding the Fluid
i	Regarding the compound i
in	At the reactor inlet, but outside the reactor
j	Regarding the Reaction j
P	Regarding the Permeate
R	Regarding the Retentate

1 Introduction

1.1 World Energy Scenario

In the past, most productive activities carried out by the society, such as agriculture, livestock, and mining, were based on manual labor. With the domestication of animals, we started to use them as transport and as tools to optimize production processes. It means that to increase the produced amount of some goods, in a generalized way, it was necessary more people, animals, and food that, even indirectly, come from solar energy. Even machines used to replace human labor, such as windmills, were based on wind energy to fulfill their purpose (Harari, 2019).

This scenario has been drastically changed since we stopped using the sustainable energy of sun and started using the chemical energy of fossil fuels, such as coal and oil, increasing the productive capacity of activities previously limited by manual labor, making them much easier and cheaper to perform (Harari, 2019).

Transport has become faster, resources extraction has become easier, the industrial revolution has become possible, which has resulted in an increase in the quality of life and life expectancy to our society. In 1965, 95% of the energy used by humanity came from fossil fuels, as illustrated in Figure 1-1.

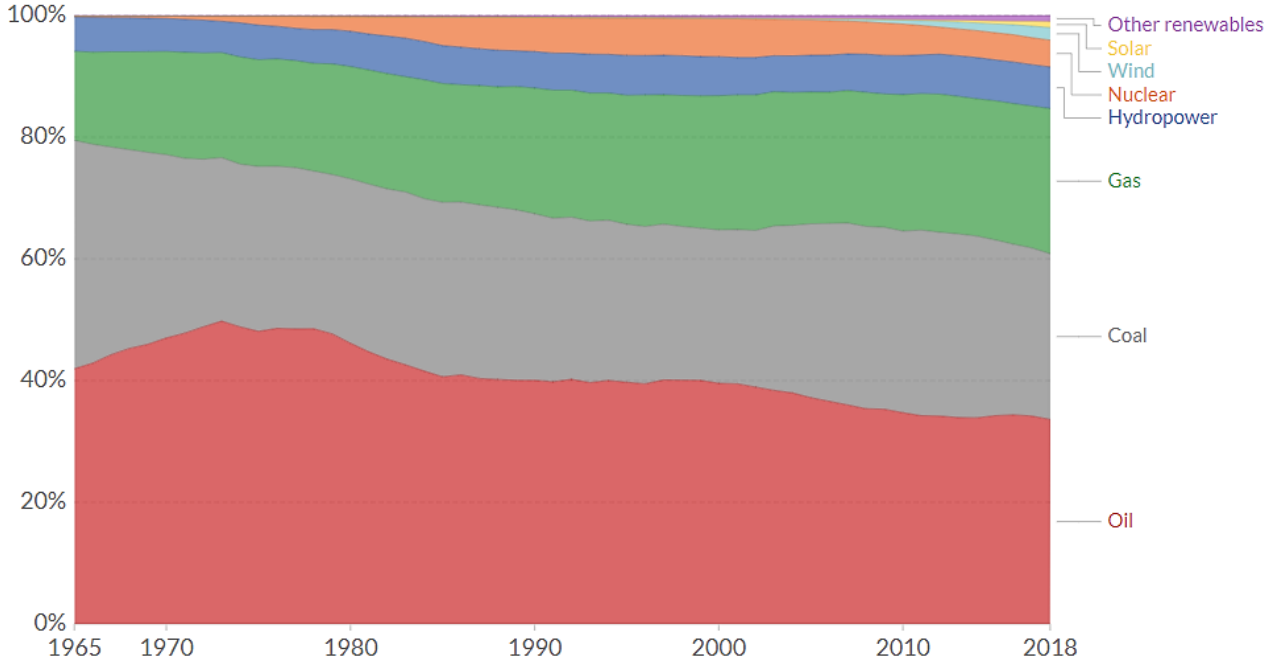

Figure 1-1. Global Energy Consumption by Source along time. Source: BP Statistical Review of World Energy (2019). Adapted from https://ourworldindata.org/energy .

But this surge in productivity brought about using fossil fuels accompanies an enormous cost that humanity is gradually becoming aware of. Since fossil fuels are obtained from extremely slow replenishing natural reserves, their extraction tends to require more and more resources and better technologies to obtain increasingly scarce and lower quality fuels. This scenario represents one of the main reasons for the unsustainability of a society based on fossil fuels and can be illustrated by the expected fall in the Energy Return on Investment (EROI) in the coming years, which consists of the quotient between the energy possible to be obtained by some source of energy in relation to the energy needed to carry out its extraction (Court & Fizaine, 2017).

In addition, even if fossil fuels could be extracted progressively at higher rates and never ran out, converting them to heat or electricity would still emit a series of compounds that contribute to the greenhouse effect, most notably carbon dioxide.

Ample physical evidence shows that carbon dioxide (CO_2) is the single most important climate-relevant greenhouse gas in Earth's atmosphere, and throughout Earth's history, there has always been a correlation between its concentration in the atmosphere and the temperature of the planet, reaching minimum values in icehouse periods and maximum values in greenhouse periods (Lacis, *et al.*, 2010).

Although these fluctuations in the concentration of CO_2 in the atmosphere are recurrent throughout history (in an interval between 200 and 300 ppm), we currently live in the period of the highest value of the last 800 thousand years, around 400 ppm, as shown in Figure 1-2 (National Oceanic and Atmospheric Administration, 2018).

Figure 1-2. Concentration of Carbon Dioxide in the Atmosphere. Source: EPICA Dome C CO_2 record (2015) and NOAA (2018). Adapted from https://ourworldindata.org/co2-and-other-greenhouse-gas-emissions .

This sudden change in the observed pattern can be explained mainly by the emission of greenhouse gases and other human activities related to the burning of fossil fuels mainly after the industrial revolution, although other factors such as variations in the behaviour of the Sun, volcanic activity and aerosols may influence this scenario in a secondary way (Hausfather, 2017). For the sake of technology and development, humanity is sending millions of tons of carbon into the air that have spent millions of years trapped beneath the Earth's surface.

In this scenario, it is proposed the development of an energy model whose excess extraction does not imply its permanent depletion, and which also does not cause significant disturbances in the biosphere in order to jeopardize the existence of the society itself. It is proposed the use of renewable energies. The representativeness of the different modalities of renewable energy consumed by humanity can be seen in Figure 1-3.

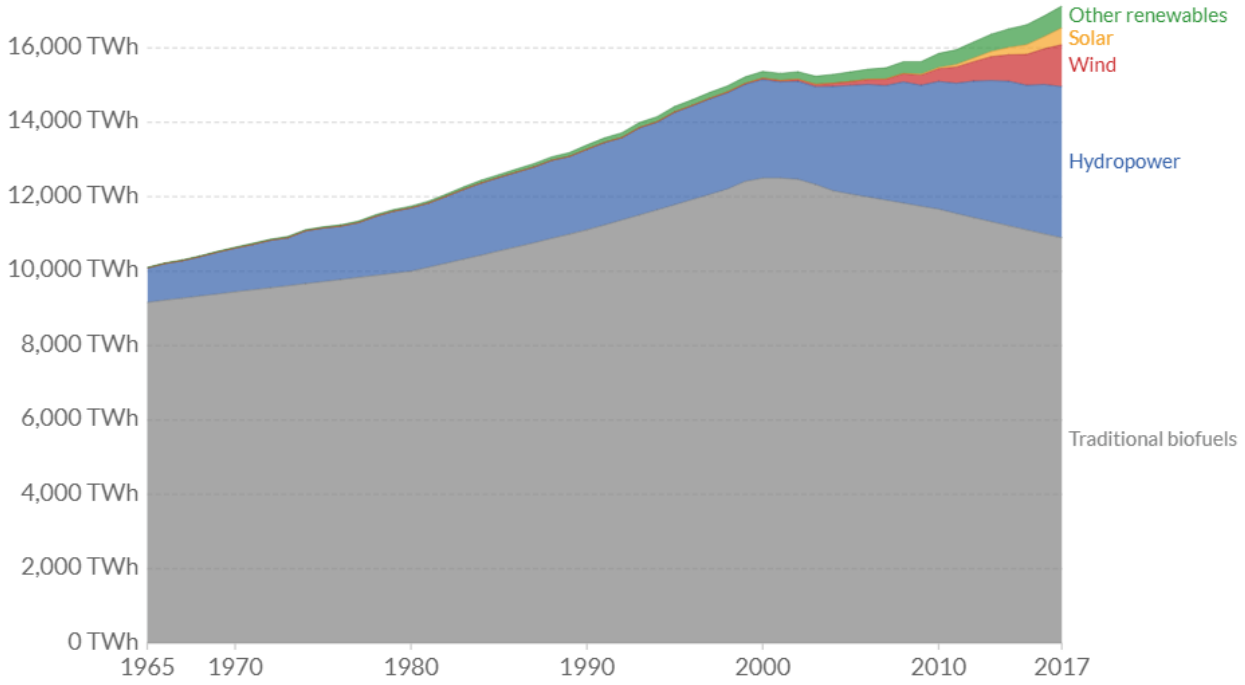

Figure 1-3. Global Consumption of Renewable Energy along time. Source: Vaclav Smil (2017) and BP Statistical Review of Global Energy (2019). Adapted from https://ourworldindata.org/renewable-energy.

Although biofuels are the main source of renewable energy used today, its production faces difficulties due to its great dependence on agriculture and forestry, causing factors such as competition from land use, erosion, loss of diversity, and possible drop in food production (Johansson, 2013); still, the metabolic limitation of plants discourages investments in this technology (Rokem & Greenblat, 2015), and for this reason, its representativeness has decreased over the recent years.

In addition, despite the fact that hydroelectric power has a very high EROI, being one of the biggest candidates to replace fossil fuels in electricity generation, its sustainability is questioned due

to the major changes caused to the regional ecosystem since it is required the interruption of river flows and frequent displacement of wildlife (Bagher, *et al.*, 2015).

Studies on the theoretical, extractable and technical potential of different sources of renewable energy show that the solar and wind power have the greatest potential to be exploited as a major energy source for the future of humanity, despite only an almost insignificant portion of this potential is used (Tsao, *et al.*, 2006).

This is mainly due to the still insufficient efficiency of the energy capture and generation process, as well as the oscillatory nature of the energy generated, requiring high synergy between its production and the energy network itself so that energy is not wasted in times of high production and that its supply is not interrupted in times of high consumption (Veers, *et al.*, 2019). In order to make the wide use of renewable energy feasible, the solution to these two problems is crucial.

1.2 Power-To-X

One of the alternatives to the above-mentioned concern of mismatch between renewable energy production and consumption is the conversion of the excess of electrical energy into chemical energy through Power-to-X technology, which consists in the production of gaseous fuels (Power-To-Gas), such as methane, or liquids (Power-To-Liquid), as methanol, using the H_2 generated by renewable energy and an external source of CO or CO_2. Particularly, the source of carbon should be CO_2 which can be captured from flue gas emitted by installations that require major burning of fossil fuels or, in the future, even from the air (Lackner, 2009).

Thus, it is possible to overcome, or at least mitigate, the intermittency problems of renewable energy sources while at the same time increasing the diversity of the energy carriers to meet the increasingly specific needs of humanity, as shown in Figure 1-4, without an excessively high capital cost since its transport and distribution could, in general, use existing infrastructures (*cf.* Figure 1-4).

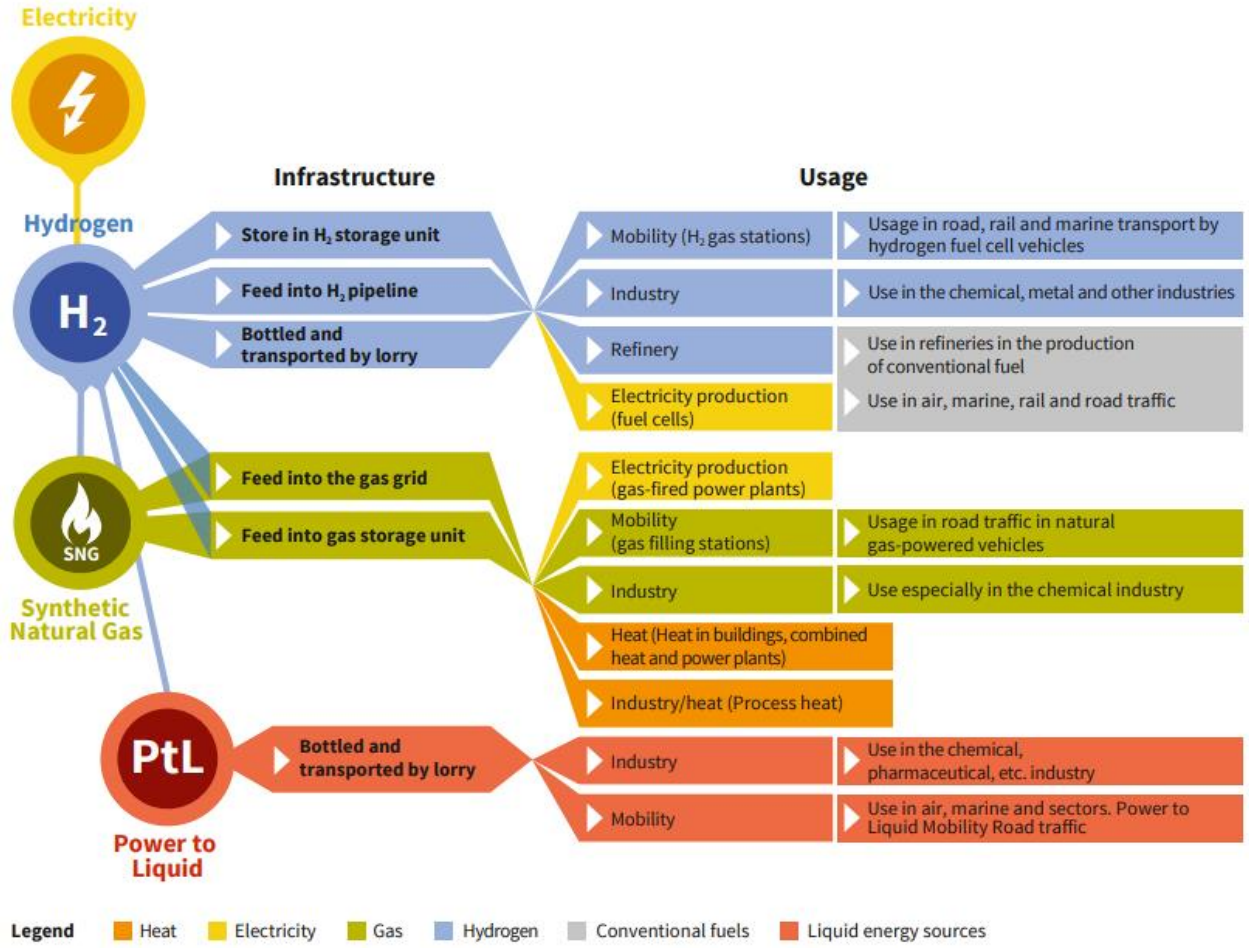

Figure 1-4. Contribution of Power-to-X technology to energy integration. Source: Deutsche Energie-Agentur (https://www.dena.de/en/topics-projects/projects/energy-systems/power-to-gas-potentiality-atlas/) .

This versatility represents one of the greatest advantages of Power-To-X technology, since it is capable of integrating the electrical and thermal energy as well as its transport and distribution for the most varied purposes, facilitating the potential of renewable energy sources to penetrate the power sector (Blanco, *et al.*, 2018). However, it is required overcoming legal and regulatory barriers, such as the maximum content fed to the gas grid of certain energy carriers like hydrogen (Dolci, *et al.*, 2019). Although this technology can be used to produce such a wide variety of fuels, two of them receive special attention in this work: methane and methanol.

At ambient conditions, methane is a gas and can be used both as a chemical feedstock and as a heat source, being the main constituent of natural gas. It presents less transportation, distribution, and storage problems when compared to H_2, and it has a better ratio of the calorific value produced to power input than methanol (Mesfun, *et al.*, 2017).

Methanol is a liquid at ambient conditions and therefore has a much higher volumetric energy density than methane and hydrogen. Because it is liquid, it also incurs minor safety problems for its use and transportation. It is a feedstock to other chemical commodities, with more than 20 million tons produced annually (Fiedler, *et al.*, 2012).

Anyway, although it is possible to make numerous comparisons between the different fuels possible to be generated through Power-To-X, it is necessary to emphasize that such comparisons should never have the objective of choosing a better-generalized solution, but rather understand the qualities and weaknesses of each solution to use them in a complementary way.

To carry out the production of these fuels, it is necessary to produce H_2 from the electrolysis of water, using the intermittent electrical energy generated by renewable energy sources. Subsequently, hydrogen gas from electrolysis is converted into methane or methanol in a catalytic (or biological) reactor by reaction with a carbon source. For the particular case of methane production (so-called Power-to-Methane), both the fuel generated and part of the hydrogen produced in the electrolysis can be inserted directly into the gas grid and redirected to several functionalities. This principle is illustrated in Figure 1-5.

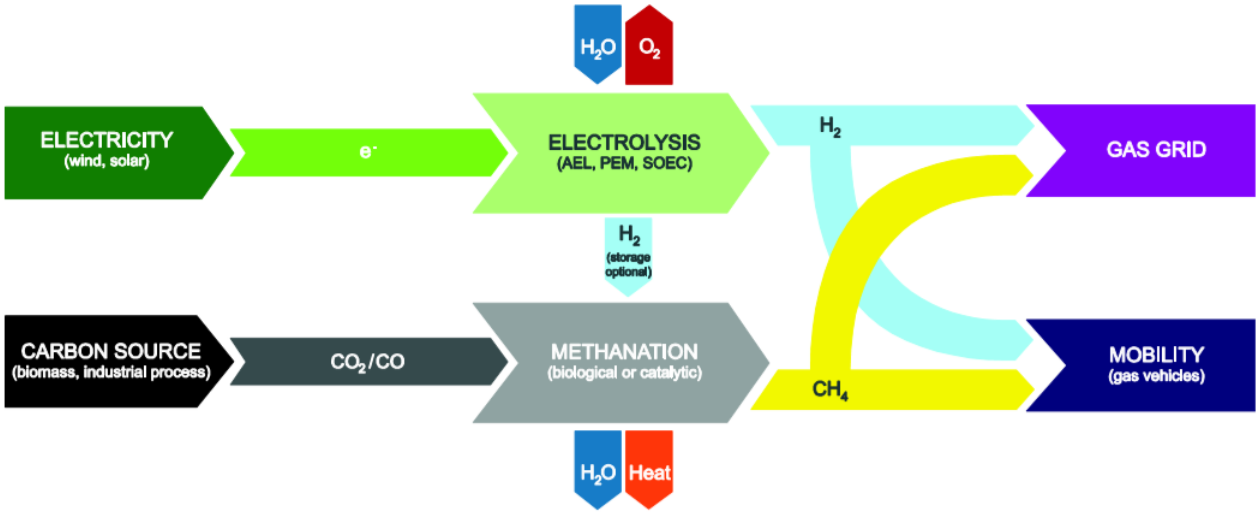

Figure 1-5. Power-to-Methane process chain. Source: *(Gotz, et al., 2016)*. Reprinted from Renewable Energy, Vol 85, Gotz, M., Lefebvre, J., Mors, F., Koch, A. M., Graf, F., Bajohr, S., Reimert, R., Kolb, T., "Renewable Power-to-Gas: A technological and economic review", Pages 1371-1390, Copyright (2016), with permission from Elsevier.

In addition to the logistical and legal problems inherent to each country, such as the gas grid infrastructure and its specifications, government support and power generation by renewable sources, the two main technical factors that limit the Power-to-Methane process are the electrolysis, capable of storing about 70% of the electrical energy generated by renewable energy sources as chemical energy (H_2), and the catalytic reactor which stores about 78% of the chemical energy of H_2 produced by electrolysis (Gotz, *et al.*, 2016).

In the catalytic reactor, the main issues to be improved are the use of the heat released by the reaction (which is partially lost) and the operational costs due to the preparation of the reactant stream to feed the reactor and in its subsequent treatment to reach the specifications necessary to be inserted into the gas grid (Gotz, *et al.*, 2016).

Regarding methanol production, in addition to the issues mentioned above, it is still necessary to mention that its chemical equilibrium implies significantly lower conversions when compared to methane, and at high temperatures it begins to suffer selectivity problems, which undermines the economic viability of its production.

In order to improve the catalytic reactor performance of either application (methane or methanol), in this work it is proposed to use a membrane reactor to remove from the catalytic bed the water produced in the hydrogenation of carbon dioxide and shift both reactions towards the products.

Thus, it would be possible to obtain conversions even greater than the chemical equilibrium based on feed composition and conditions (and therefore higher quantities of product with the same amount of reactants) or to obtain the same conversions, but under softer conditions (and therefore reduce operational costs), which ultimately can contribute for improving the efficiency of Power-to-X processes.

1.3 Objectives and Outline

The main objective of this work is to understand the effect of intensive process variables in the production of methane and methanol through the hydrogenation of CO_2, as well as the potential of this process by using membrane reactors.

To achieve this goal, it was used as a starting point a MATLAB program developed at LEPABE capable of simulating the hydrogenation of CO_2 into methane inside a traditional fixed-bed reactor or a membrane reactor considering the mathematical model detailed in section 3. This program was rewritten maintaining the original equations of its model and its numerical resolution methodology (function *bvp4c*), but it was generalized for any set of gaseous chemical reactions (including simultaneous), and now may involve an unlimited number of species (as long as their physical properties are known). These properties are stored in an Excel file and can be re-accessed by the MATLAB script for any further simulation. So, the program is no longer limited to the study of methane production and it allows the study of any other known gas-phase catalytic reaction, such as CO_2 hydrogenation to methanol.

For the simulation of the membrane reactor, experimental data from a hydrophilic sodalite (SOD) membrane were used (Wang, *et al.*, 2014) and extrapolated for both CO_2 hydrogenation reactions conditions. The validation of kinetics found in the literature for the production of methane (Falbo, *et al.*, 2018) and methanol (Portha, *et al.*, 2017) was firstly carried out, followed by the simulation of numerous different scenarios for traditional and membrane reactors, in an interval between 250 – 410 °C and 1 – 7 atm for methane and between 150 – 310 °C and 10 – 70 atm for methanol.

For both compounds, the influence of pressure and temperature for traditional and membrane reactors was evaluated. Then, the influence of the permeate feed and of the pressure ratio between the permeate and the retentate chambers was evaluated for membrane reactors.

Since it was also considered the feed of reactants simultaneously in the retentate and permeate, it was then discussed the impact of those changes in the product yield for a membrane reactor. Different performance indexes were proposed, as detailed below in section 3.4, from the perspective of the whole operational unit and from the perspective of the catalytic bed only.

Finally, the effect of the pressure ratio between the permeate and retentate streams in a specific case where all reactants which remained in the permeate were completely separated and recycled, thus reducing the amount of reactants needed to feed the system.

2 State of The Art

2.1 Reactions and Catalysts

Although over many years Zn/CrO catalysts have been used in the production of methanol, at temperatures between 300 – 400 °C and pressures between 250 – 350 atm, these materials presented problems related to selectivity, resulting in a considerable amount of secondary products such as methane and other hydrocarbons (Lange, 2001). Since the 1960s, Cu/ZnO catalysts have become the most used in this process, making possible operation in softer conditions, such as those carried out by Imperial Chemical Industries and Lurgi Ol-Gas-Chemie GmbH (about 250 °C and 50 atm) (Palma, *et al.*, 2018).

Even though today they are the most used in the production of methanol from the hydrogenation of CO_2, Cu/ZnO catalysts present deactivation problems, especially at high temperatures and in the presence of water (Fichtl, *et al.*, 2015).

The production of methanol occurs through a complex mechanism, exhaustively discussed elsewhere (Graaf, *et al.*, 1986; Graaf, *et al.*, 1988) , which is currently believed to be described in three main steps: the Hydrogenation of CO_2 in methanol (Eq. 2.1); the transformation of CO_2 into CO, known as Water-Gas-Shift reaction (Eq. 2.2); and the hydrogenation of CO in methanol (Eq. 2.3) (Portha, *et al.*, 2017);

$$CO_2 + 3H_2 \leftrightarrow CH_3OH + H_2O \qquad \Delta H\ (298\ \text{K}) = -49.4\ \text{kJ/mol} \qquad \text{Eq. 2-1}$$

$$CO_2 + H_2 \leftrightarrow CO + H_2O \qquad \Delta H\ (298\ \text{K}) = 41.1\ \text{kJ/mol} \qquad \text{Eq. 2-2}$$

$$CO + 2H_2 \leftrightarrow CH_3OH \qquad \Delta H\ (298\ \text{K}) = -90.5\ \text{kJ/mol} \qquad \text{Eq. 2-3}$$

As for the production of methane, the use of Ni/Al_3O_2 catalysts is common, due to the high selectivity and low cost (Martins, *et al.*, 2019). Alternatively, it is possible to choose Ru/Al_3O_2 catalysts, which in addition to higher selectivity have a higher resistance to oxidation. In this case, it is necessary to accept its higher cost (Miguel, *et al.*, 2018).

Similarly, methane production can be represented through the CO_2 hydrogenation reaction (Eq. 2-4) (Falbo, *et al.*, 2018):

$$CO_2 + 4H_2 \leftrightarrow CH_4 + 2H_2O \qquad \Delta H\ (298\ \text{K}) = -165\ \text{kJ/mol} \qquad \text{Eq. 2-4}$$

In both cases, the reactions responsible for the production of methanol and methane (2-1; 2-3; 2-4) are exothermic and promote a decrease in the number of moles of the gaseous compounds. According to Le Chatelier's principle, this makes it necessary to operate at low temperatures and high

pressures to obtain higher equilibrium conversions and so promote, from the thermodynamic point of view, the production of methane and methanol. On the other hand, low temperatures can impair the reaction rate, requiring longer contact times between the reactants and the catalyst to achieve higher conversions.

Finally, it is crucial to control the heat generated by these reactions, which will not only contribute to shift the balance against the products but also represent possible energy losses in a process whose main objective is the chemical storage of energy.

2.2 Configurations to Improve the Temperature Profile

In order to mitigate the increase in temperature during the production of methane and methanol, keeping it high enough to be kinetically satisfactory but low enough to be thermodynamically viable, some ideas commonly applied around the world are illustrated in Figure 2-1.

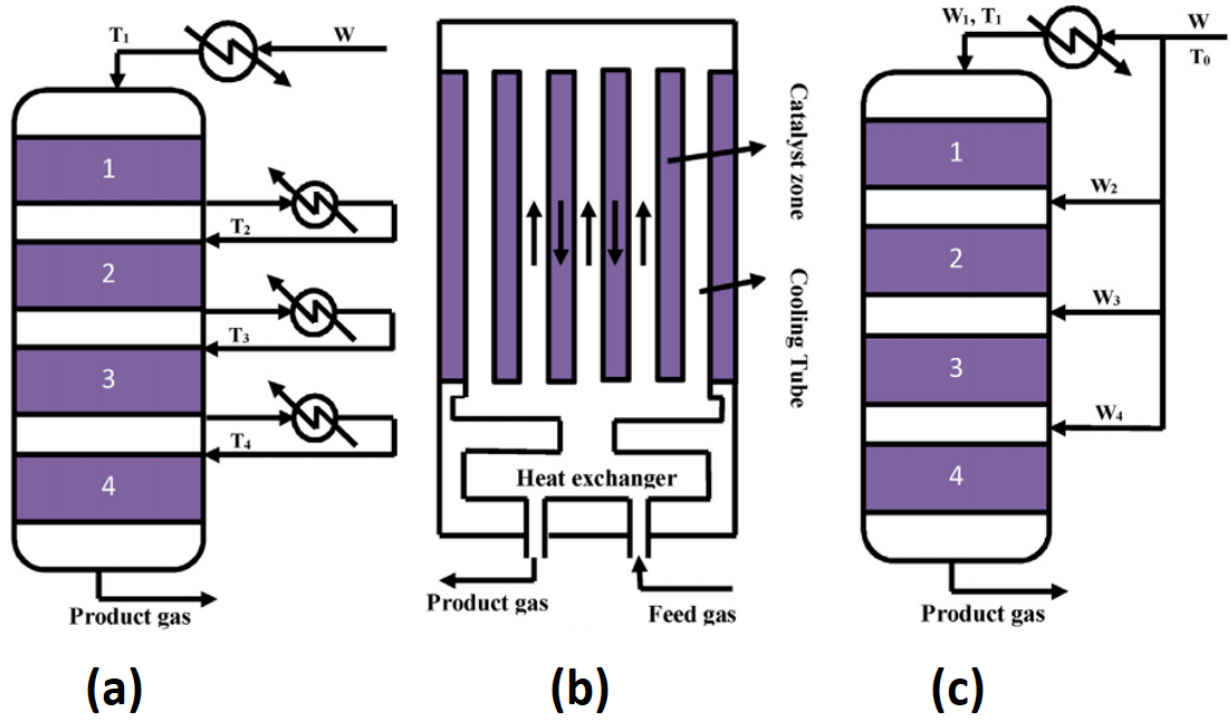

Figure 2-1. Diagram of (a) adiabatic indirect cooling reactor, (b) internal direct cooling reactor, (c) adiabatic quench cooling reactor. Adapted from: *(Khademi & Sabbaghi, 2017)*. Reprinted from Chemical Engineering Research and Design, Vol 128, Khademi, M. H. & Sabbaghi, R. S., "Comparison between three types of ammonia synthesis reactor configurations in terms of cooling methods", Pages 306-317, Copyright (2017), with permission from Elsevier.

One of the most common, due to its simplicity, is the use of coolers between several adiabatic reactors in series (Figure 2-1(a)), wherein for each reactor the compounds would reach equilibrium and then are cooled in order to shift the chemical equilibrium forward and allow the formation of

larger quantities of products, while the heat removed can be used for several other needs of the factory.

It is also possible to make use of polytropic reactors, designed in a similar way to shell and tube heat exchangers, where the tubular reactors would be surrounded by a cold fluid and then making temperature control more effective (Figure 2-1(b)). This process was proposed by Lurgi Ol-Gas-Chemie GmbH with the aim of being able to produce methanol in milder conditions than those used by Imperial Chemical Industries. However, they have relatively high costs and have a production capacity limited by the size of the shell (Palma, *et al.*, 2018).

Another alternative is the Quench Reactor (Figure 2-1(c)), where only part of the feed is preheated and the remaining is fed cold throughout the reactor, shifting the equilibrium without the use of fluids with an exclusively thermal purpose (Santangelo, *et al.*, 2008). One of the disadvantages of this technology is that the feed inserted along the reactor will have shorter contact time with the catalytic bed, in addition to resulting in a significantly more complex system to be operated, involving the control of several streams whose flow, pressure and temperature will interact with each other throughout the reactor (Griffiths, 1984).

2.3 Configurations to Improve the Concentration Profile

Finally, multifunctional reactors can be mentioned, which propose (among other possibilities) the separation of compounds along the reactor through principles such as adsorption or separation by membranes, unifying reaction and separation in a single process unit, which can reduce operating costs and increase the yield of products (Rodrigues, *et al.*, 2017). Thus, such reactors propose to shift the chemical equilibrium mainly by changing the concentration of components in the reactive medium instead of changes in temperature as in the cases previously mentioned.

In the case of adsorptive reactors, the bed is formed by a mixture of catalyst and adsorbent, so that the first is responsible for the chemical reaction and the second for the in-situ adsorption of one or more formed products, shifting the reaction forward, i.e. favoring of the products.

The unit is operated in two steps: i) the reaction phase, where the reactants are fed at the inlet, the products are obtained in the outlet and one of the products is adsorbed to the solid phase; and ii) the regeneration phase, either by pressure or temperature swing, where the adsorbate is removed from the adsorbent bed. This procedure is illustrated in Figure 2-2.

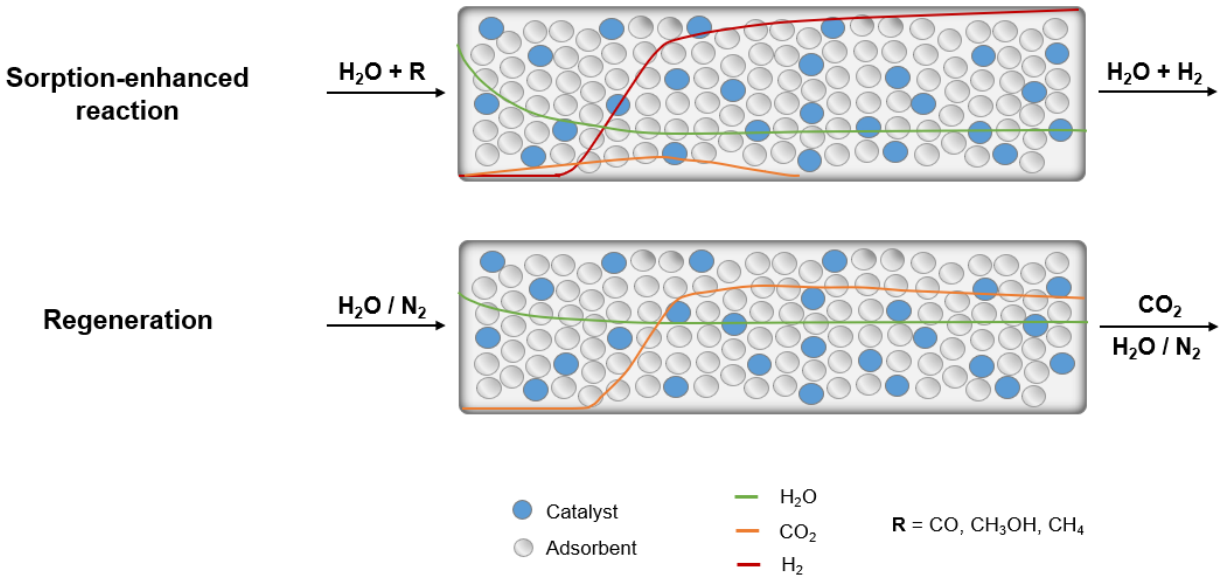

Figure 2-2. Hydrogen production with adsorptive reactors: (A) sorption-enhanced reaction step and (B) adsorbent regeneration step.

Since an adsorption-enhanced reactor unit requires two discrete steps to accomplish its purpose, in continuous processes at least two units are required, always operating in opposite phases. It is currently one of the most promising areas of study in chemical reaction engineering and its main challenges rely on the development of adsorbent materials compatible with the catalyst (because they should operate under the same conditions) as well as the optimization of the cyclic nature of its operation.

For membrane reactors, the bed is commonly surrounded by a concentric tubular membrane, as shown in Figure 2-3. The chosen membrane can be organic (polymeric) or inorganic (metallic, ceramic, carbonic, zeolitic). The choice depends on the conditions of the reaction, selectivity, capital, and operational costs.

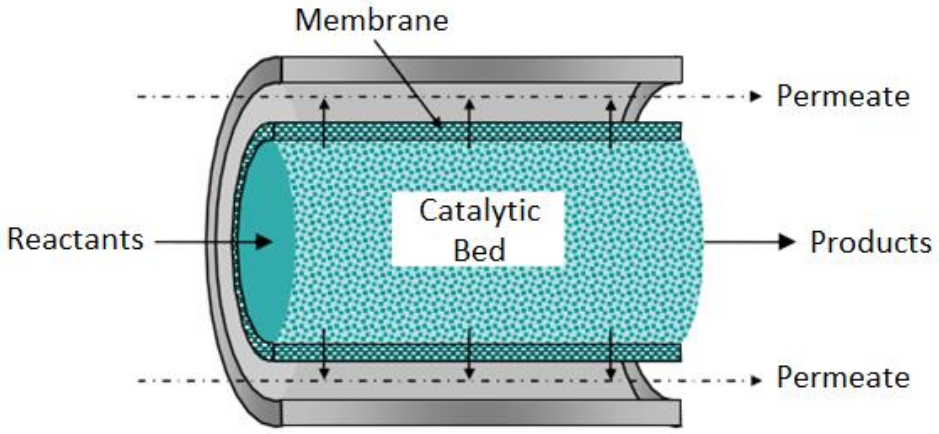

Figure 2-3. Scheme of a Membrane Reactor. Adapted from *(Gonçalves, 2011)*.

Polymeric membranes have high versatility in their preparation resulting in the potential to achieve greater performance in some specific processes. On the other hand, due to problems inherent to their own nature, they are more vulnerable to heat, pH, and chemical degradation (Vital & Sousa, 2013).

On the other hand, inorganic membranes can tolerate high temperatures and chemically harsh environments that are very common in most processes of industrial relevance. For this reason, inorganic membranes are more used for processes such as the production of methane and methanol.

In general, the membrane is responsible for permeating only one or two compounds involved in the process and can be used for (i) removing a given product, in order to shift the chemical equilibrium towards the products side or (ii) controlling the addition of reactants to the catalytic bed in a way to distribute it evenly throughout the reactor while removing a desired intermediate product, being especially useful in situations where high concentrations of a certain reactant can impair the selectivity of the process. Both scenarios are illustrated in Figure 2-4.

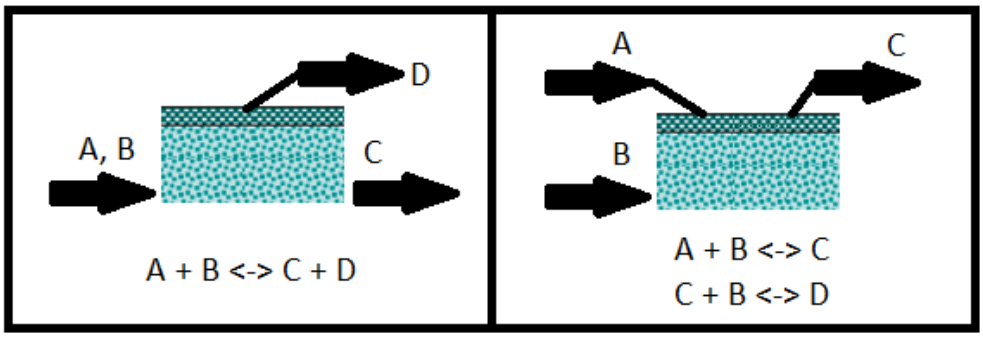

Figure 2-4. Two possible approaches to membrane reactors.

Thus, membrane reactors can be used to obtain higher yields of the desired product either through (i) greater conversions of the reactant(s) or (ii) greater selectivity to the desired product.

3 Model

3.1 Traditional Reactor

In this work, the simulations focused on two reactor configurations. The first one, the traditional reactor, is composed of a fixed-bed tubular reactor packed with a catalyst. The system is placed inside a furnace, where the temperature is always constant.

The model is not dynamic, so the reactor is assessed at steady-state. The pressure drop along the reactor is described according to the Ergun equation in which the bed porosity (ε_b) is constant. The model follows a one-dimensional pseudo-homogeneous plug flow hypothesis with axial dispersion, where all gases have an ideal behavior.

All simulations used 200 intervals through the reactor length. Data related to the equilibrium curves, calculated based on feed conditions, were obtained using Aspen Plus software, through the minimization of Gibbs' free energy method. Finally, all systems of differential equations were solved using the MATLAB function *bvp4c*, which was released with MATLAB 6.0 to solve ordinary differential equations (ODE) and its tutorial can be found in literature (Kierzenka, 2016).

The equations and boundary conditions of the traditional reactor are the following (please refer to the Notation and Glossary section for the meaning of each variable):

Partial mass balance for species *i*

$$\frac{\varepsilon_b\, D_{\mathrm{ea}}}{L^2}\,\frac{d^2 C_{i,\mathrm{b}}}{\mathrm{d}z^2} - \frac{\mathrm{d}\left(u_0\, C_{i,\mathrm{b}}\right)}{L\,\mathrm{d}z} + \sum_j \rho_{\mathrm{b}}\, \alpha_{i,j}\, \Re_j{}' = 0 \qquad \text{Eq. 3-1}$$

Energy balance

$$\frac{\lambda_{\mathrm{ea}}}{L^2}\,\frac{\mathrm{d}^2 T_b}{\mathrm{d}z^2} - \frac{u_0\,\rho_f}{L}\,\frac{\mathrm{d}\left(T_b\, C_{p,f}\right)}{\mathrm{d}z} + \sum_j \rho_{\mathrm{b}}\,(-\Delta H)\,\Re_j{}' - \frac{2\,U}{r}(T_{\mathrm{b}} - T^{\infty}) = 0 \qquad \text{Eq. 3-2}$$

Total mass balance

$$\frac{\mathrm{d}\left(u_0\, C_{i,\mathrm{b}}\right)}{L\,\mathrm{d}z} - \sum_j \rho_{\mathrm{b}} \sum_i (\alpha_{i,j})\ \Re_j{}' = 0 \qquad \text{Eq. 3-3}$$

Momentum balance

$$\frac{\mathrm{d}P}{\mathrm{d}z} = -L\left(150\,\frac{(1-\varepsilon_{\mathrm{b}})^2\,\mu_{\mathrm{f}}}{{\varepsilon_{\mathrm{b}}}^3\,{d_{\mathrm{p}}}^2}u_0 + 1.75\,\frac{(1-\varepsilon_{\mathrm{b}})\,\rho_{\mathrm{f}}}{{\varepsilon_{\mathrm{b}}}^3\,d_p}\,{u_0}^2\right) \qquad \text{Eq. 3-4}$$

Boundary conditions

z=0

$$\frac{\mathrm{d}C_{i,\mathrm{b}}}{\mathrm{d}z} = -\frac{u_0\, L}{\varepsilon_\mathrm{b}\, D_\mathrm{ea}}\left(C_{i,\mathrm{b}}^{\mathrm{in}} - C_{i,\mathrm{b}}\right); \frac{\mathrm{d}T_b}{\mathrm{d}z} = -\frac{u_0\, \rho_\mathrm{f}\, C_{p,\mathrm{f}}\, L}{\lambda_\mathrm{ea}}\left(T^{\mathrm{in}} - T_\mathrm{b}\right);$$

$$P^{\mathrm{in}} = P\,;\, u_0^{\mathrm{in}} = u_0$$

Eq. 3-5 – 3-8

z=1

$$\frac{\mathrm{d}C_{i,\mathrm{b}}}{\mathrm{d}z} = 0\,;\, \frac{\mathrm{d}T_\mathrm{b}}{\mathrm{d}z} = 0$$

Eq. 3-9 – 3-10

3.2 Membrane Reactor

The second configuration, the membrane reactor, is composed of a catalytic bed with the same assumptions made in the traditional reactor. However, this catalytic bed is enclosed by a tubular membrane that separates the reactor in two zones: the retentate and the permeate. The system is also placed inside a furnace, where the temperature is always constant. This scheme of the membrane reactor is illustrated in Figure 3-1.

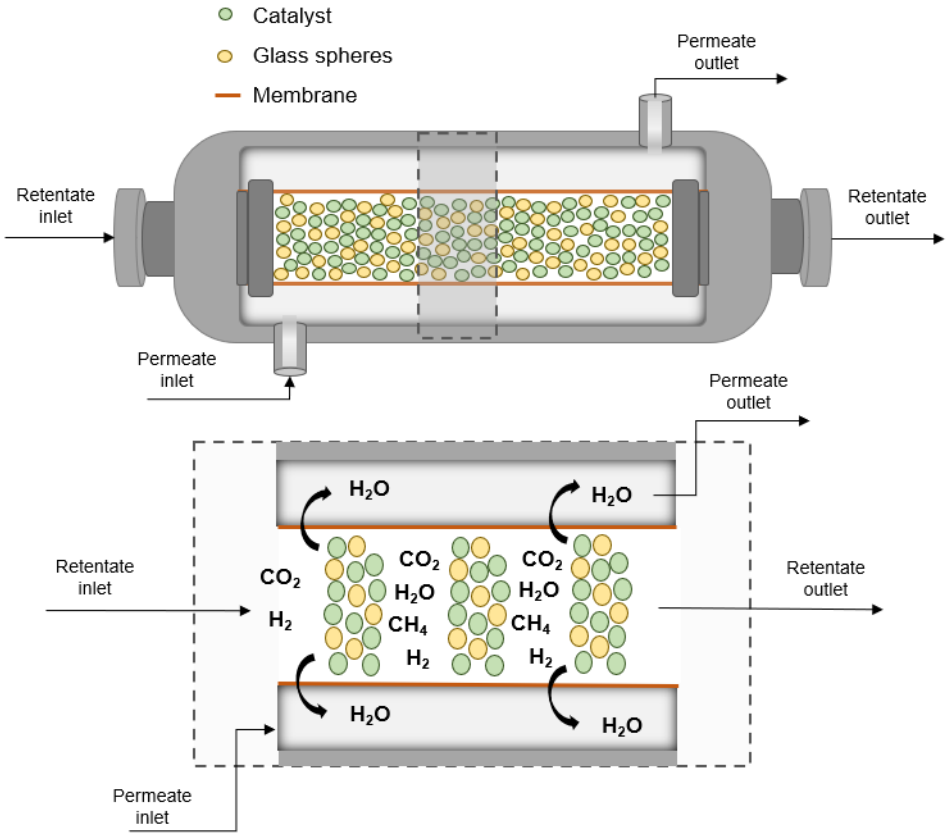

Figure 3-1 – Scheme of the membrane reactor simulated in this work (sweep gas flowing co-currently).

The reactions can occur only at the retentate chamber, where the catalytic bed is placed. The permeate is the annular chamber between the membrane and the outer reactor wall, fed with a sweep gas flowing co-currently to the reacting mixture. In the permeate it is considered an ideal plug-flow behavior with no pressure drop. The equations and boundary conditions of the membrane

reactor are the following (please refer to the Notation and Glossary section for the meaning of each variable):

Retentate

Partial mass balance for species *i*

$$\frac{\varepsilon_{\mathrm{b}} \cdot D_{\mathrm{ea}}^{\mathrm{R}}}{L^2} \cdot \frac{\mathrm{d}^2 {C_{i,\mathrm{b}}}^{\mathrm{R}}}{\mathrm{d}z^2} - \frac{\mathrm{d}\left({u_0}^{\mathrm{R}} \cdot {C_{i,\mathrm{b}}}^{\mathrm{R}}\right)}{L \cdot \mathrm{d}z} + \sum_j {\rho_{\mathrm{b}}}^{\mathrm{R}} \cdot \alpha_{i,j} \cdot {\Re_j}' - \frac{2 \cdot \pi \cdot r^{\mathrm{R}}}{A^{\mathrm{R}}} J_i = 0 \qquad \text{Eq. 3-11}$$

Energy balance

$$\frac{{\lambda_{\mathrm{ea}}}^{\mathrm{R}}}{L^2} \cdot \frac{\mathrm{d}^2 {T_{\mathrm{b}}}^{\mathrm{R}}}{\mathrm{d}z^2} - \frac{{u_0}^{\mathrm{R}} \cdot {\rho_{\mathrm{f}}}^{\mathrm{R}}}{L} \frac{\mathrm{d}\left({T_{\mathrm{b}}}^{\mathrm{R}} \cdot {C_{p,\mathrm{f}}}^{\mathrm{R}}\right)}{\mathrm{d}z} + \sum_j \rho_{\mathrm{b}} \cdot \left(-\Delta H_j\right) \cdot {\Re_j}' - \frac{2 \cdot \pi \cdot r^{\mathrm{R}}}{A^{\mathrm{R}}} \left[U^{\mathrm{R}} \cdot \left({T_{\mathrm{b}}}^{\mathrm{R}} - {T_{\mathrm{b}}}^{\mathrm{P}}\right) + \sum_i \left(J_i \cdot {C_{p,i}}^{\mathrm{R}}\right) \cdot \left({T_{\mathrm{b}}}^{\mathrm{R}} - {T_{\mathrm{b}}}^{\mathrm{P}}\right) \right] = 0 \qquad \text{Eq. 3-12}$$

Total mass balance

$$\frac{\mathrm{d}\left({u_0}^{\mathrm{R}} \cdot {C_{i,\mathrm{b}}}^{\mathrm{R}}\right)}{L \cdot \mathrm{d}z} - \sum_j {\rho_{\mathrm{b}}}^{\mathrm{R}} \cdot \sum_i \left(\alpha_{i,j}\right) \cdot {\Re_j}' + \frac{2 \cdot \pi \cdot r^{\mathrm{R}}}{A^{\mathrm{R}}} \cdot J_i = 0 \qquad \text{Eq. 3-13}$$

Momentum balance

$$\frac{\mathrm{d}P^{\mathrm{R}}}{\mathrm{d}z} = -L \cdot \left(150 \cdot \frac{(1-\varepsilon_{\mathrm{b}})^2 \cdot {\mu_{\mathrm{f}}}^{\mathrm{R}}}{{\varepsilon_{\mathrm{b}}}^3 \cdot {d_{\mathrm{p}}}^2} \cdot {u_0}^{\mathrm{R}} + 1.75 \cdot \frac{(1-\varepsilon_{\mathrm{b}}) \cdot {\rho_{\mathrm{f}}}^R}{{\varepsilon_{\mathrm{b}}}^3 \cdot d_{\mathrm{p}}} \cdot {u_0}^{\mathrm{R}^2} \right) \qquad \text{Eq. 3-14}$$

Boundary conditions

z=0

$$\frac{\mathrm{d}{C_{i,\mathrm{b}}}^{\mathrm{R}}}{\mathrm{d}z} = -\frac{{u_0}^{\mathrm{R}} \cdot L}{\varepsilon_{\mathrm{b}} \cdot D_{\mathrm{ea}}} \cdot \left(C_{i,\mathrm{b}}^{\mathrm{R,in}} - {C_{i,\mathrm{b}}}^{\mathrm{R}}\right);$$

$$\frac{\mathrm{d}{T_{\mathrm{b}}}^{\mathrm{R}}}{\mathrm{d}z} = -\frac{{u_0}^{\mathrm{R}} \cdot {\rho_{\mathrm{f}}}^{\mathrm{R}} \cdot {C_{p,\mathrm{f}}}^{\mathrm{R}} \cdot L}{\lambda_{\mathrm{ea}}} \cdot \left(T^{\mathrm{R,in}} - {T^{\mathrm{R}}}_{\mathrm{b}}\right); \quad P^{\mathrm{R,in}} = P^{\mathrm{R}}; \quad u_0^{\mathrm{R,in}} = {u_0}^{\mathrm{R}}; \qquad \text{Eq. 3-15 – 3-18}$$

z=1

$$\frac{\mathrm{d}{C_{i,\mathrm{b}}}^{\mathrm{R}}}{\mathrm{d}z} = 0\,; \; \frac{\mathrm{d}{T_{\mathrm{b}}}^{\mathrm{R}}}{\mathrm{d}z} = 0 \qquad \text{Eq. 3-19 – 3-20}$$

Permeate

Partial mass balance for species *i*

$$\frac{\mathrm{d}\left({u_0}^{\mathrm{P}} \cdot {C_{i,\mathrm{b}}}^{\mathrm{P}}\right)}{L \cdot \mathrm{d}z} = -\frac{2 \cdot \pi \cdot r^{\mathrm{R}}}{A^{\mathrm{P}}} \cdot J_i \qquad \text{Eq. 3-21}$$

Energy balance

$$\frac{{u_0}^{\mathrm{P}} \cdot {\rho_{\mathrm{f}}}^{\mathrm{P}}}{L} \cdot \frac{\mathrm{d}\left({T_{\mathrm{b}}}^{\mathrm{P}} \cdot {C_{p,\mathrm{f}}}^{\mathrm{P}}\right)}{\mathrm{d}z} \cdot \frac{A^{\mathrm{P}}}{2 \cdot \pi} =$$

$$\left[r^{\mathrm{R}} \cdot U^{\mathrm{R}} \cdot \left({T_{\mathrm{b}}}^{\mathrm{R}} - {T_{\mathrm{b}}}^{\mathrm{P}}\right) + r^{\mathrm{R}} \cdot \sum_i \left(J_i \cdot {C_{p,i}}^{\mathrm{P}}\right) \left({T_{\mathrm{b}}}^{\mathrm{R}} - {T_{\mathrm{b}}}^{\mathrm{P}}\right) - r^{\mathrm{P}} \cdot U^{\mathrm{P}} \cdot \left({T_{\mathrm{b}}}^{\mathrm{P}} - T^{\infty}\right)\right] \quad \text{Eq. 3-22}$$

Total mass balance

$$\frac{\mathrm{d}\left({u_0}^{\mathrm{P}} \cdot {C_b}^{\mathrm{P}}\right)}{L \cdot \mathrm{d}z} = -\frac{2 \cdot \pi \cdot r^{\mathrm{R}}}{A^{\mathrm{P}}} \cdot \sum_i J_i \quad \text{Eq. 3-23}$$

Boundary conditions

z=0 $\quad {C_{i,\mathrm{b}}}^{\mathrm{P}} = \frac{y_i^{\mathrm{P}} \cdot P^{\mathrm{P}}}{R \cdot T^{\mathrm{P}}}; \quad P^{\mathrm{P,in}} = P^{\mathrm{P}}; \quad T^{\mathrm{P,in}} = {T^{\mathrm{P}}}_{\mathrm{b}}; \quad u_0^{\mathrm{P,in}} = {u_0}^{\mathrm{P}};$ Eq. 3-24 – 3-27

Molar Flux Through the Membrane

$$J_i = {Perm_i}^{\mathrm{R}} \cdot \left(p_i^{\mathrm{R}} - p_i^{\mathrm{P}}\right) \quad \text{Eq. 3-28}$$

3.3 Membrane Data Extrapolation

The permeance parameters of a hydrophilic sodalite (SOD) membrane were taken from the literature (Wang, *et al.*, 2014). The authors prepared the membrane and determined experimentally its permeance between 125 °C and 200 °C for water, hydrogen, methane, and methanol. The permeance dependence on the absolute temperature is assumed of the Arrhenius-type (Eq. 3-29) and its parameters were estimated through regression of Eq. 3-29 after linearization. Estimated parameters of Eq. 3-29 for each species are listed in Table 3-1.

$$Permeance = \beta \cdot \exp\left(\frac{-E_a}{R \cdot T}\right) \quad \text{Eq. 3-29}$$

Table 3-1. Pre-exponential factor (β) and $E_a \cdot R^{-1}$ for calculating the membrane permeance as a function of temperature for the different species.

	β (mol m^{-2} s^{-1} Pa^{-1})	$E_a \cdot R^{-1}$ (K^{-1})
CH_3OH	$5.84 \cdot 10^{-10}$	$9.27 \cdot 10^{1}$
H_2O	$7.86 \cdot 10^{-8}$	$8.23 \cdot 10^{1}$
H_2	$9.71 \cdot 10^{-7}$	$1.60 \cdot 10^{3}$
CO_2	$6.99 \cdot 10^{-6}$	$3.26 \cdot 10^{3}$
CH_4	$5.39 \cdot 10^{-7}$	$1.84 \cdot 10^{3}$

In Figure 3-2, circles represent the experimental data collected from the literature (Wang, et al., 2014) and the continuous lines shows the permeance estimated at different temperatures.

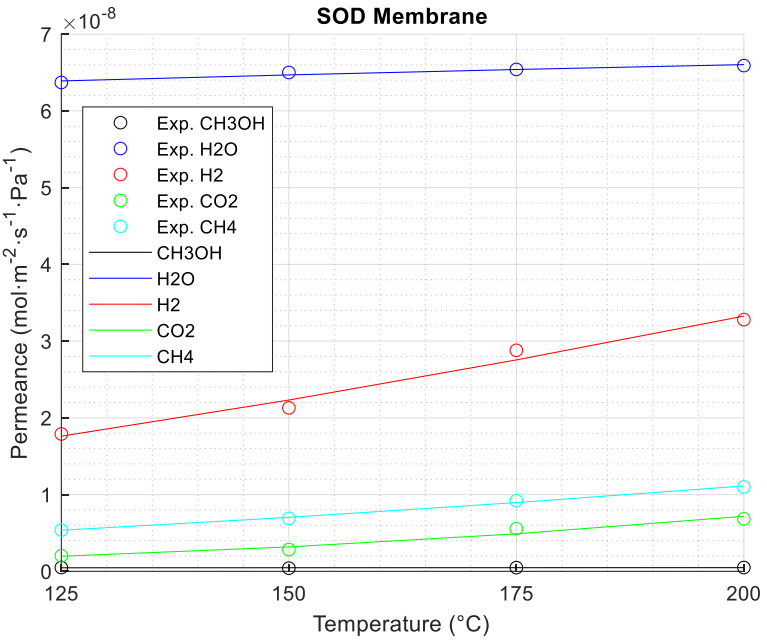

Figure 3-2. The permeance of the referred hydrophilic SOD membrane as a function of temperature. Continuous lines represent the model obtained through regression using Eq. 3-29 and circles represent the experimental data collected from the literature *(Wang, et al., 2014)*.

Also, it was possible to estimate the permeance of the referred membrane at kinetically viable temperatures for the production of methane (between 250 °C and 410 °C) and methanol (between 210 °C and 270 °C), through an extrapolation of the data, as shown in Figure 3-3.

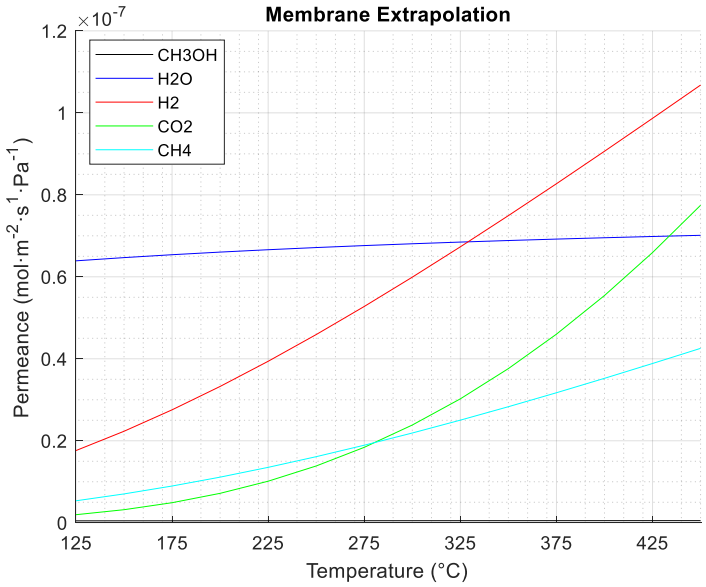

Figure 3-3. Membrane permeance as a function of temperature. Values calculated through the regression described in Eq. 3-29 and parameters shown in Table 3-1.

It is important to note that at higher temperatures, water permeance starts to become less and less significant when compared to the permeance of other compounds, such as CO_2 and H_2, whose apparent activation energies for permeation are much higher (cf. Table 3-1); for methane this would

also occur, but at higher temperatures due to its smaller pre-exponential factor. This may cause a problem with the loss of reactants and of the desired product (particularly for the case of methane) along the catalytic bed when using a water-selective membrane reactor, decreasing the CO_2 conversion and product purity. On the other hand, if the system is operating at lower temperatures to avoid this, the conversion may deteriorate due to slower reaction rates.

The permeance of CH_4 also increases, with the result that part of the produced species (in a power-to-methane process) may be mixed with the permeate stream. This is not observed with methanol, whose permeance remains very low, according to the extrapolation that has been made (as a result of the extremely low pre-exponential factor, β - cf. Table 3-1).

3.4 Reactor Performance Indicators

Since in several examples of this work both the permeate and retentate streams are fed with CO_2 (and also H_2, for the reasons detailed later on), there are two approaches to consider about the conversion definition (i.e. amount of CO_2 converted per amount of fed CO_2) or even the yield of an arbitrary product (amount of product in the outlet streams per amount of fed CO_2). To help explaining these two approaches please consider Figure 3-4 for guidance.

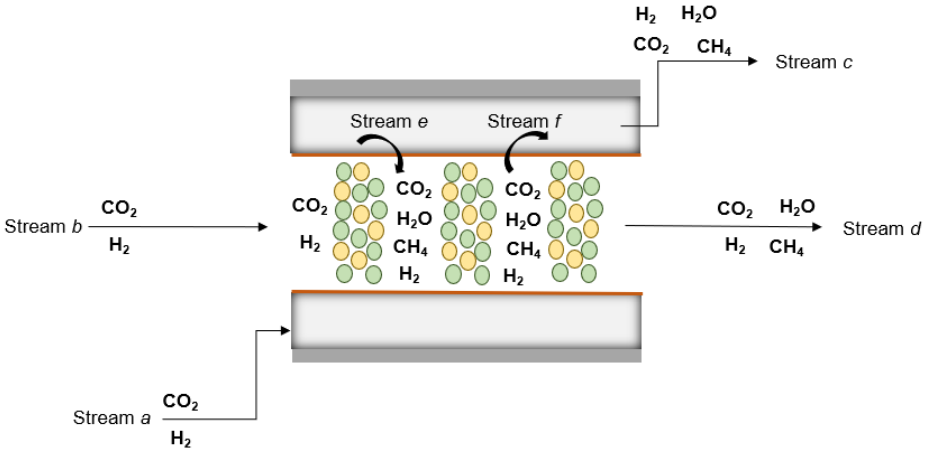

Figure 3-4. Scheme illustrating the streams used approach of system and catalytic bed to calculate CO_2 conversion and the yield of an arbitrary product. All comparisons between TR and MR utilize the same molar feed of reactants.

The first one considers the **whole system** (retentate and permeate) as the basis for calculation, according to Equations 3-30 and 3-31.

$$System\ CO_2\ Conversion = \frac{(F_{CO_2,a} + F_{CO_2,b}) - (F_{CO_2,c} + F_{CO_2,d})}{(F_{CO_2,a} + F_{CO_2,b})} \qquad \text{Eq. 3-30}$$

$$System\ Yield\ of\ i = \frac{(F_{i,c} + F_{i,d}) - (F_{i,a} + F_{i,b})}{(F_{co_2,a} + F_{co_2,b})} \qquad \text{Eq 3-31}$$

In this case, it is possible to compare the efficiency of two units (traditional reactor – TR - versus membrane reactor - MR) in converting CO_2 or producing an arbitrary product, *i*. This approach makes it simpler to compare the results of these two units (TR and MR) being fed with the same molar flow rate just by comparing the System CO_2 conversion with the conversion of a traditional reactor which is fed with $F_a + F_b$. However, this index is strongly influenced by the molar flux of reactants permeating through the membrane since even if the catalytic bed could convert all CO_2 in the retentate, that index would not be 1 unless all CO_2 fed in the permeate moves to the retentate. Therefore, a higher system conversion does not necessarily imply better process economics since factors such as the easiness of recovering reactants and products should be taken into account. This index represents, however, the best choice to compare two units if there is no viable way to recover any reactant of its outlet streams.

The second option is to consider only the **catalytic bed as the basis for calculation**, accordingly with Eq. 3-32 and Eq. 3-33.

$$CO_2\ Conversion\ of\ the\ Catalytic\ Bed = \frac{(F_{CO_2,e} + F_{CO_2,b}) - (F_{CO_2,f} + F_{CO_2,d})}{(F_{CO_2,e} + F_{CO_2,b})} \qquad \text{Eq. 3-32}$$

$$Yield\ of\ i\ of\ the\ Catalytic\ Bed = \frac{(F_{i,f} + F_{i,d}) - (F_{i,e} + F_{i,b})}{(F_{co_2,e} + F_{co_2,b})} \qquad \text{Eq. 3-33}$$

In this case, it is possible to compare the efficiency of two bulks in converting CO_2 by comparing the CO_2 conversion of the catalytic bed and the CO_2 conversion of a traditional reactor fed with $F_e + F_b$. It is very difficult to know the exact amount of F_e (i.e., fed in the permeate chamber but moving radially towards the retentate along the reactor length), making the comparison with a traditional reactor with the same molar feed flow rate very difficult in practice, especially in cases where there are both entries and exits of reactants at different positions of the catalytic bed. However, in this work, it is possible to know the exact amount fed radially since it is a simulated reactor[1].

Despite this index does not necessarily represent the capacity of the whole unit to convert CO_2, it is quite useful to analyze how efficient the reactor (as definition, where the chemical reaction occurs) is in transforming reactants into products. For traditional reactors, the Catalytic Bed and System Conversion (and Yield of a product) are the same since the catalytic bed does represent the whole system. It also can be observed mathematically comparing Eq. 3-32 and Eq. 3-33 with Eq. 3-30 and Eq. 3-31, considering that in a traditional reactor, the streams a, c, e, and f are not existent.

[1] The molar flow rates of CO_2 and H_2 through the membrane were integrated only for negative values (streams from the permeate zone to the catalytic bed) in order to know the amount of reactants that entered the bed radially (F_e).

Finally, since all studied cases of methanol production carried out in this work using membrane reactors presented a permeate stream mainly composed by reactants and water, it is useful to define a third index, the **Global Yield of Methanol**. This index is calculated as the ratio of the amount of methanol captured on the retentate outlet stream over the amount of CO_2 needed to feed the system if all the reactants present in the permeate outlet stream are completely recovered, separated (by simple steam condensation) and recycled. This concept is illustrated in Figure 3-5 and described by Eq. 3-34.

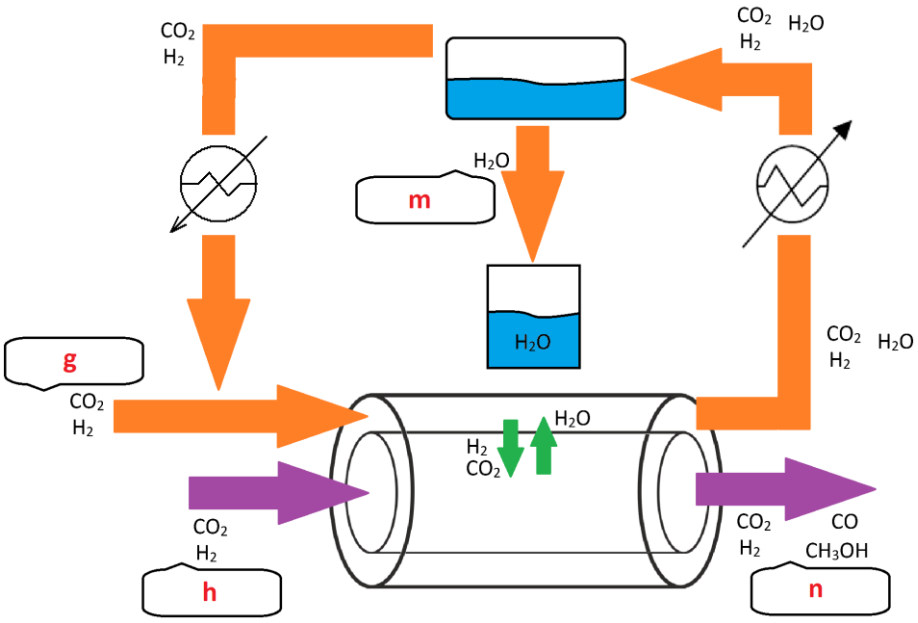

Figure 3-5. Scheme illustrating the approach of Global Yield of Methanol - global inlet and outlet. The inlet streams (g *and* h) are set to supplement the exact amount of H_2 and CO_2 to keep the system feed streams, at reactor entrance, equal. If necessary, the recycled stream can feed both retentate and permeate.

$$Global\ Yield\ of\ Methanol = \frac{(F_{i,\mathrm{n}}) - (F_{i,\mathrm{g}} + F_{i,\mathrm{h}})}{(F_{co_2,\mathrm{g}} + F_{\mathrm{co_2,h}})} \qquad \text{Eq. 3-34}$$

All comparisons must be made with a traditional reactor fed with the same molar feed of reactants needed to supply the membrane reactor ($F_{\mathrm{g}} + F_{\mathrm{h}}$). This way, it is possible to compare the difference between feeding a certain amount of reactants in a membrane reactor with permeate recycling and feeding the same amount of reactants in a traditional reactor.

The highest difference is that the Global Yield of Methanol besides considering the yield of the catalytic bed also considers the benefits in the existence of reactants on the permeate outlet stream, which, expectably, are easy to recover. However, this index does not consider that this recovery has a cost, and therefore it is useful whenever permeate recovery is easy/inexpensive. As with any other index, it must be analyzed critically.

3.5 Physical Properties

In order to estimate the model parameters (D_{ea}^{R}, ${\lambda_{ea}}^{R}$, ${C_{p,f}}^{R}$ and ${\mu_f}^{R}$) it is necessary to calculate the physical properties of the compounds in the fluid mixture and of the fluid mixture itself. The scheme utilized to make these estimatives are represented in Figure 3-6.

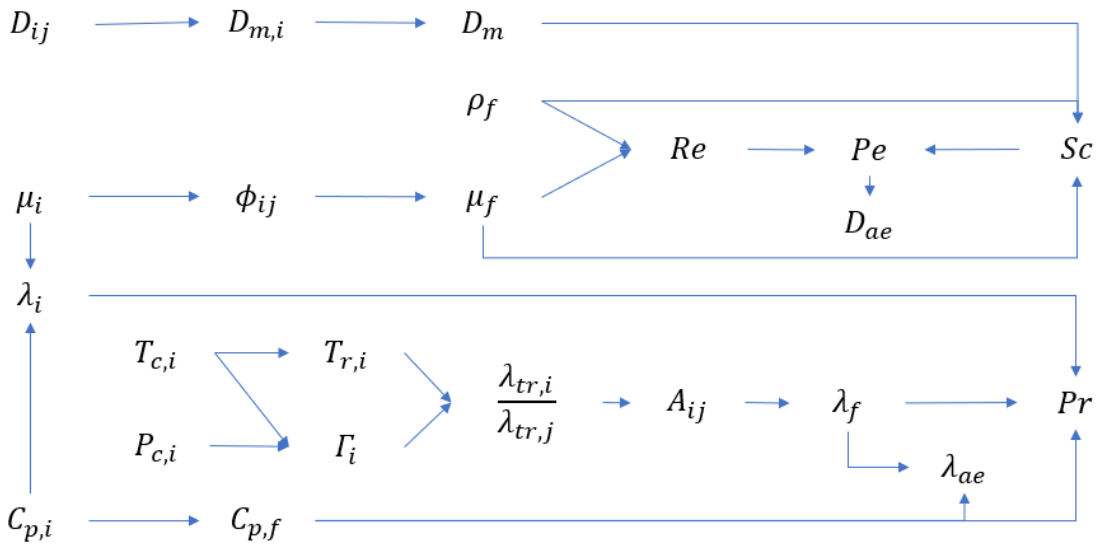

Figure 3-5. Scheme to estimate the dimensionless numbers of the fluid mixture: Reynolds (*Re*), Peclet (*Pe*), Schmidt (*Sc*), and Prandtl (*Pr*).

This method utilizes thermodynamic properties such as the molar heat capacity ($C_{p,i}$) and viscosity (μ_i) of each species as a function of temperature, the molecular diffusion ($D_{m,i}$) and the critical temperature ($T_{c,i}$) and pressure ($P_{c,i}$) as a basis to estimate all other parameters.

All equations and thermodynamic data necessary to estimate these values are presented in Appendix A (all information necessary about the meaning of every variable is presented in the referred appendix).

To determine U^{R} and U^{P}, the global coefficients for heat transfer from the retentate to the permeate and from the permeate to the furnace, respectively, it was necessary to estimate the thermal resistance of the catalytic bed, of the membrane, of the permeate zone, and the natural convection outside the reactor (but inside the furnace). This method is described in Appendix B.

Every propriety was calculated and updated in each iteration and calculated locally, as a function of the mixture composition and temperature and pressure conditions.

4 Results and Discussion

4.1 CO_2 Conversion Into Methane

4.1.1 Kinetic Model Validation

In order to assess the ability of the computational model to represent reality satisfactorily, some experiments published by other authors were simulated and the results compared.

For methane formation, the kinetic law was based on the article by Falbo *et al*. (Falbo, *et al.*, 2018), which proposes a kinetic model for a 0.5 wt.% Ru/γ-Al_2O_3 commercial catalyst, operated inside a fixed-bed reactor whose characteristics are shown in Table 4-1.

Table 4-1. Characteristics of the reactor utilized to obtain the experimental data *(Falbo, et al., 2018)*.

Length (cm)	23
Internal Diameter (mm)	11
Catalyst Particles Diameter (μm)	80
Catalyst Mass (mg)	375

A series of experiments were carried out by the authors in the ranges described in Table 4-2. The output stream was analyzed by gas chromatography and, accordingly to the authors, in none of the tests traces of C_{2+} hydrocarbons were observed.

Table 4-2. Experimental conditions utilized to obtain the experimental data *(Falbo, et al., 2018)*.

Temperature (°C)	250-410
Pressure (atm)	1-7
Space Velocity $(\mathbf{L_{STP} \cdot h^{-1} \cdot g_{cat}^{-1}})$	3.75-10.00
H_2/CO_2 Inlet Ratio (mol_{H2}/mol_{CO2})	1-5

The constants determination was performed by modeling an isothermal homogeneous plug-flow reactor and the kinetic law suggested by those authors is represented in Equations 4-1 – 4-3 (wherein the subscript 2.4 refers to Equation 2-4, i.e., the methanation reaction):

$$\Re'_{2.4} = \frac{1000 \cdot k_{2.4}}{1 + 0.91 \cdot p_{H_2O}} \cdot \left\{ \left[\frac{p_{CO_2}}{1.01325}\right]^{0.152} \cdot \left[\frac{p_{H_2}}{1.01325}\right]^{0.608} - \frac{\left[\frac{p_{CH_4}}{1.01325}\right]^{0.152} \cdot \left[\frac{p_{H_2O}}{1.01325}\right]^{0.304}}{(K_{2.4})^{0.152}} \right\} \quad \text{Eq. 4-1}$$

$$k_{2.4} = 95.43 \cdot \exp\left(\frac{-75300}{R \cdot T}\right) \quad \text{Eq. 4-2}$$

$$\ln K_{2.4} = \left(\frac{1}{1.987}\right) \cdot \left(\frac{56000}{T^2} + \frac{34633}{T} - 16.4 \cdot \ln T + 0.00557 \cdot T\right) + 33.165 \qquad \text{Eq. 4-3}$$

All experiments involving methane formation in the present work consider this kinetic law. In order to validate it, a set of simulations were executed between 250 °C and 410 °C, at atmospheric pressure, with a volumetric flow rate of 31.25 $mL_{STP} \cdot min^{-1}$ (which represents a space velocity of 5 $L_{STP} \cdot h^{-1} \cdot g_{cat}{}^{-1}$). The molar contents in the feed stream, as in the original paper, were 18% CO_2, 72% H_2, and 10% N_2. The reactor dimensions and catalyst information were replicated as well.

The CO_2 conversion was determined and compared with those obtained experimentally (Falbo, *et al.*, 2018), and the results are shown in Figure 4-1.

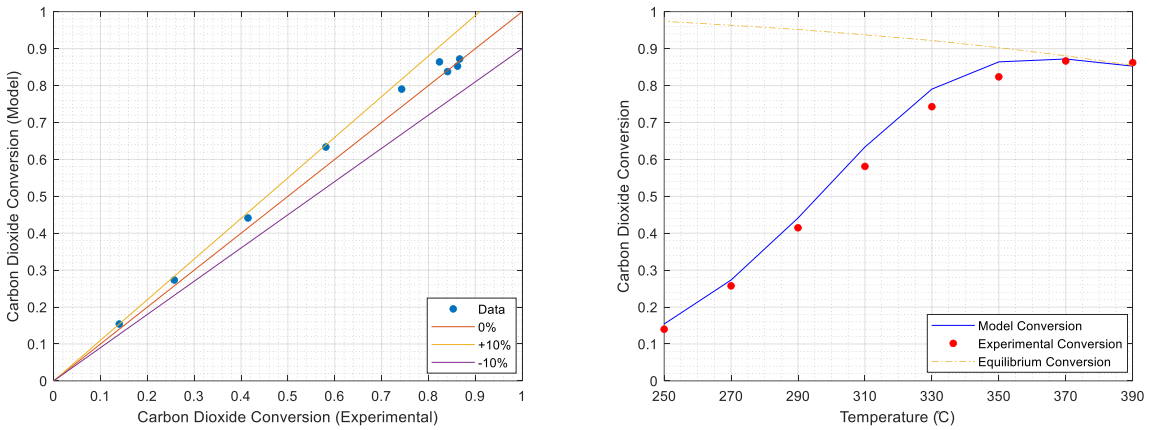

Figure 4-1. Comparison between the data obtained through the kinetic model used in this work and the data obtained experimentally *(Falbo, et al., 2018)*. (a) Parity plot; (b) Carbon dioxide conversion as a function of temperature.

In general, it is possible to observe that the model developed herein presents conversions slightly above to those observed experimentally (i.e. in the original paper). This can be explained by the fact that the authors used an isothermal homogeneous plug-flow reactor to model the kinetic constants. Thus, when using the same constants in a non-isothermal reactor, the results are expectedly superior in temperatures where the conversion is limited by kinetics since the heat released will increase the reaction rate. Despite this, it is possible to note that the model satisfactorily predicts results (+/- 10% uncertainty), particularly at higher temperatures, where the conversion approaches the equilibrium.

4.1.2 Traditional Reactor: Overview

In this section, a reactor with the same characteristics as the one used in (Falbo, *et al.*, 2018) was simulated with a feed stream at 395 °C, 1 atm, and with a space velocity of 20 $L_{STP} \cdot h^{-1} \cdot g_{cat}^{-1}$. These conditions of temperature and pressure were chosen because they are commonly used in the production of methane (Gotz, *et al.*, 2016) . The molar content of the feed stream is 20% CO_2 and 80%

H_2, just like in all other methane production simulations performed in this work. The concentration, temperature, and molar flow rate profiles are shown in Figure 4-2.

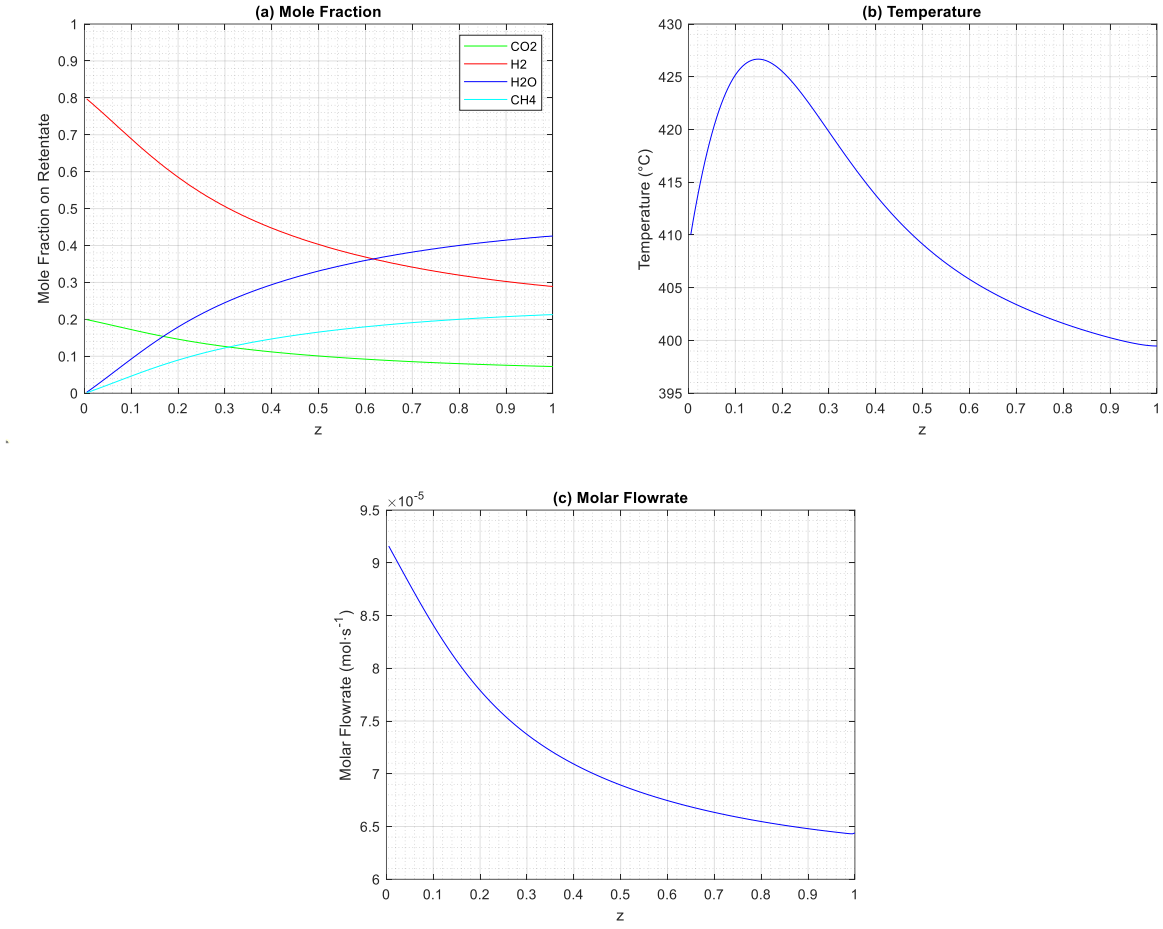

Figure 4-2. Data obtained for a Traditional Reactor with the characteristics presented in Table 4-1. Feed stream conditions of 395 °C and 1 atm with a space velocity of 20 $L_{STP} \cdot h^{-1} \cdot g_{cat}^{-1}$.

This is probably one of the simplest cases presented in this work, and so it is extremely useful as a starting point to discuss the most basic characteristics, without the interference of variables such as a membrane with different pressures through it, or even multiple reactions in the catalytic bed. In addition, it will also serve as a benchmark to be surpassed by the membrane reactor configurations proposed to produce methane.

In Figure 4-2(a), it is possible to notice the increase of products and decrease of reactants molar fraction, according to the stoichiometric proportion of methanation reaction (Eq. 2-4). The traditional reactor presented a conversion of CO_2 of 74.6% (for a traditional reactor, the System Conversion (Eq. 3-30) is equal to the Catalytic Bed Conversion (Eq. 3-32) for the reasons explained in Section 3.4).

Also, in Figure 4-2(b) is possible to observe a hot spot caused by the heat released by this strongly exothermic reaction, whose peak is located in the zone where the reaction rate slows down so that it cannot generate more heat than is lost through the reactor walls. Finally, despite the feed

temperature being 395 °C, the graph shows the curve starting at 410 °C. That difference occurs due to Danckwert's boundary conditions (Eq. 3-16).

To evaluate the conversion dependencies of pressure and temperature in the feed stream, a series of simulations were carried out, with a space velocity of $5\ L_{STP} \cdot h^{-1} \cdot g_{cat}^{-1}$, and all other conditions remaining the same as in Figure 4-2. The results are shown in Figure 4-3.

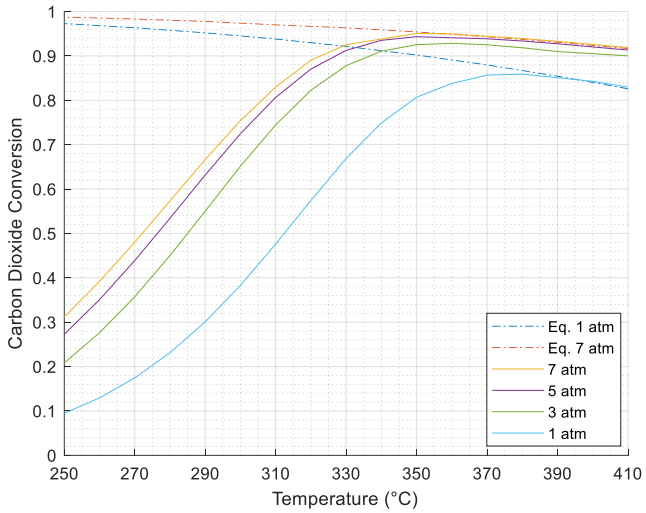

Figure 4-3. X_{CO_2} obtained for different conditions of temperature and pressure on the feed stream, for a Traditional Reactor. The reactor characteristics are presented in Table 4-1. The feed stream for all simulations had a space velocity of 5 $L_{STP} \cdot h^{-1} \cdot g_{cat}^{-1}$. The model is represented by continuous lines, while thermodynamic equilibrium conversions are represented by dashed-dot lines.

As expected, both temperature and pressure are responsible to increase the reaction rate; under mild conditions, the conversion of CO_2 increases with either of these parameters because it is limited mainly by the kinetic factor.

At higher temperatures, reaction kinetics becomes progressively less relevant when compared to the limit imposed by the chemical equilibrium, up to a point where the increase of feed temperature spoils CO_2 conversion (since it shifts the chemical equilibrium of the exothermal reactions to make less product). The opposite occurs with the increase of the feed pressure, since it shifts the equilibrium to the side with the fewer number of moles of gas, producing higher amounts of products (this behavior can be observed comparing the dashed-dot lines in Figure 4-3).

Therefore, using a lower space velocity than in previous simulations allowed to validate equilibrium curves obtained with Aspen Plus (please see in Fig. 4-3 that that model curves approaches the corresponding equilibrium curve when the temperature increases).

4.1.3 Membrane Reactor with N_2 as Sweep-Gas

In this section, the use of a membrane is proposed to separate water from the catalytic bed. Decreasing the concentration of this product in the reaction medium shifts the reaction towards

greater methane production. The goal is to obtain higher CO_2 conversions (potentially higher than the chemical equilibrium) or else equally satisfactory conversions but in milder conditions when compared to a traditional packed-bed reactor, reducing the operational costs.

Therefore, to start analyzing the magnitude of improvement that a membrane reactor can provide for methane production, a reactor with the same bed and feed stream specifications considered for results shown in Figure 4-2 was simulated, but including the above described hydrophilic sodalite (SOD) membrane. The ratio between the pressure at permeate feed and the pressure at retentate feed will be defined as pressure ratio, which for this case study was chosen as 2/3, feeding the permeate with an N_2 stream at 0.666 atm. The results are presented in Figure 4-4.

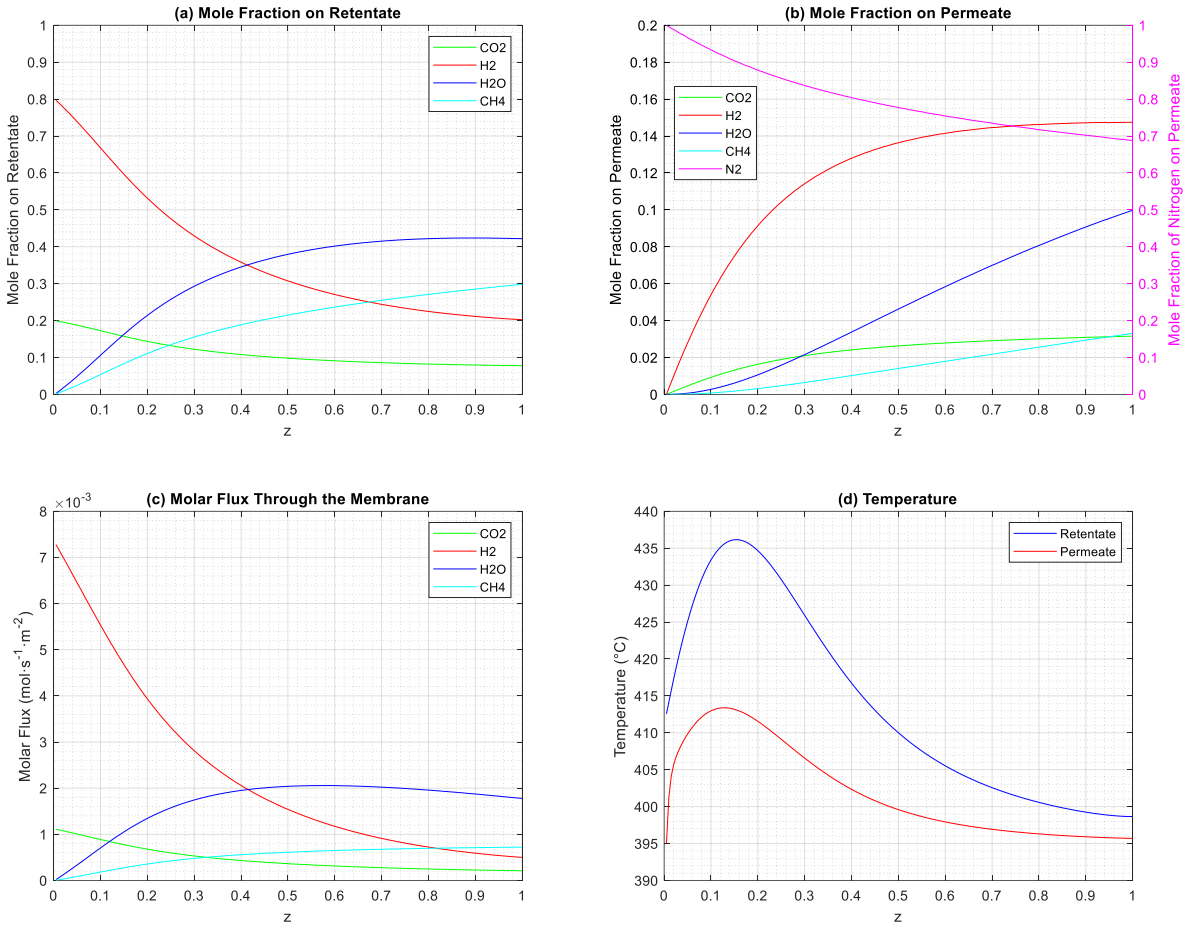

Figure 4-4. Data obtained for a Membrane Reactor with the characteristics presented in Table 4-1. Feed streams with a space velocity of 20 $L_{STP} \cdot h^{-1} \cdot g_{cat}^{-1}$ and conditions of 395 °C and 1 atm (retentate) or 0.666 atm (permeate).

The membrane reactor presented a CO_2 conversion of 66.1% which is significantly lower than the 74.6% presented by the traditional reactor. As observed in Figure 4-4(c), it occurred mainly because a huge part of reactants permeated through the membrane before they could even react, mixing with N_2 and causing its molar fraction to decrease from 1 to approximately 0.70 as a result of dilution, as shown in Figure 4-4(b). The permeation of water through the membrane is not sufficient

to compensate for the loss of reactants. In fact, the total amount of H_2 which permeated was even higher than H_2O, deviating completely from the main objective.

Additionally, despite the total amount of CH_4 produced was lower than in the traditional reactor, and so the total amount of heat released, the temperature on the retentate was slightly higher, as can be observed comparing Figure 4-4(d) and Figure 4-2(d). It occurred because the permeate stream (and even the permeate-furnace wall) are adding up two more resistances to the heat transfer. It is also noteworthy that despite both permeate and retentate are fed at the same temperature, the permeate is modeled as a plug-flow unit and so the temperature at the start is the same as the feed temperature, while the retentate has axial dispersion (and so Danckwert's boundary conditions).

In an attempt to reduce the permeance of CO_2 and mainly H_2, another simulation was made but considering the retentate feed stream at 300 °C instead of 395 °C; the idea behind was to improve membrane selectivity towards steam, as can be inferred from Fig. 3-2. The results are shown in Figure 4-5.

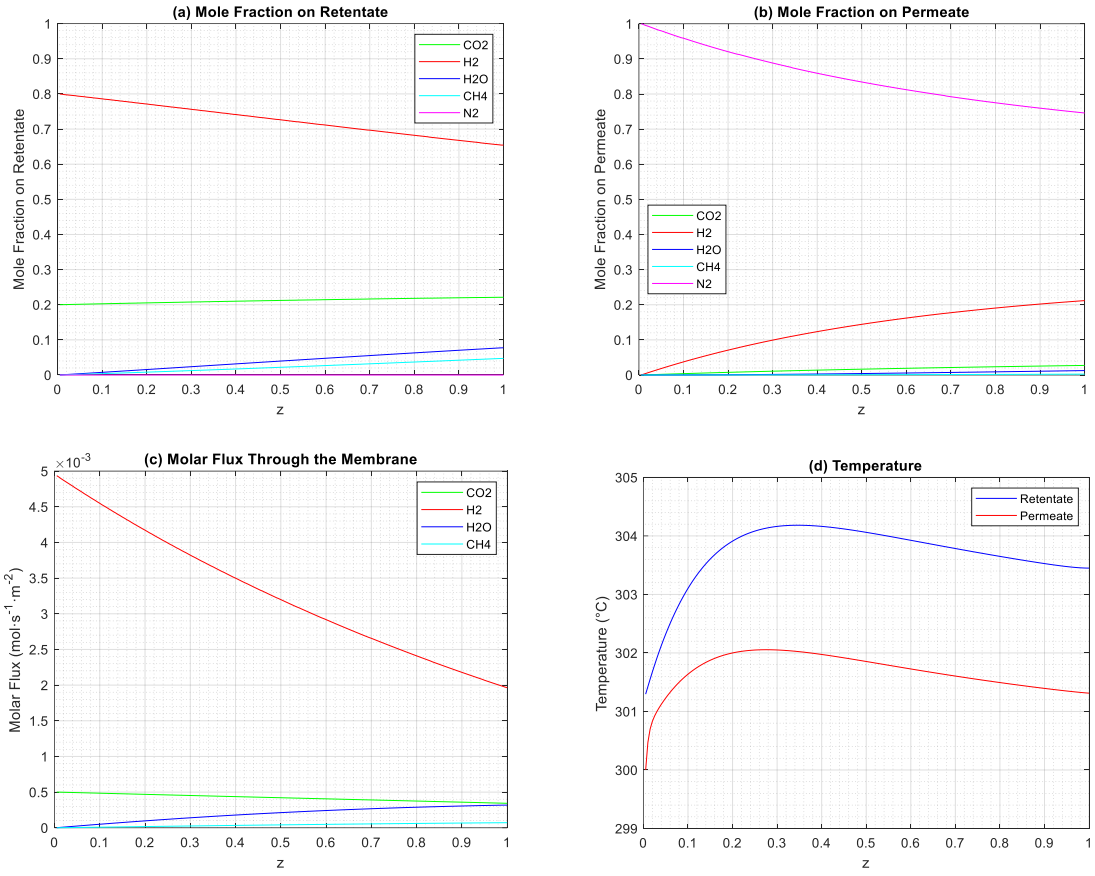

Figure 4-5. Data obtained for a Membrane Reactor with the characteristics presented in Table 4-1. Feed streams with a space velocity of 20 $L_{STP} \cdot h^{-1} \cdot g_{cat}^{-1}$ and conditions of 300 °C and 1 atm (retentate) or 0.666 atm (permeate).

In Figure 4-5(c) and Figure 4-5(b), it is possible to observe that the loss of reactants decreased when compared with Figure 4-4(c) and Figure 4-4(b). However, the methanation kinetics

was strongly affected, reducing the CO_2 conversion from 66.1% to 15.8% (calculated using data presented in Figure 4-5(a)). Such decrease of the reaction rate can also be observed in the temperatures profile, Figure 4-5(d), where the temperature at retentate increases only about 4 °C from feed to the hottest point, versus 42 °C in the previous case.

Then, since the greatest limitations observed were the high permeance of CO_2, H_2, and also CH_4 at kinetically viable temperatures for the reaction, a simulation was performed using fictitious parameters of a membrane which has the same permeance to water as the hydrophilic SOD membrane but null permeance towards all other compounds; this represents an ideal membrane, with infinite permselectivity towards the desired component (water in this case), as occurs for instance with some H_2-selective Pd-based membranes (Rodrigues, *et al.*, 2017). The results are shown in Figure 4-6.

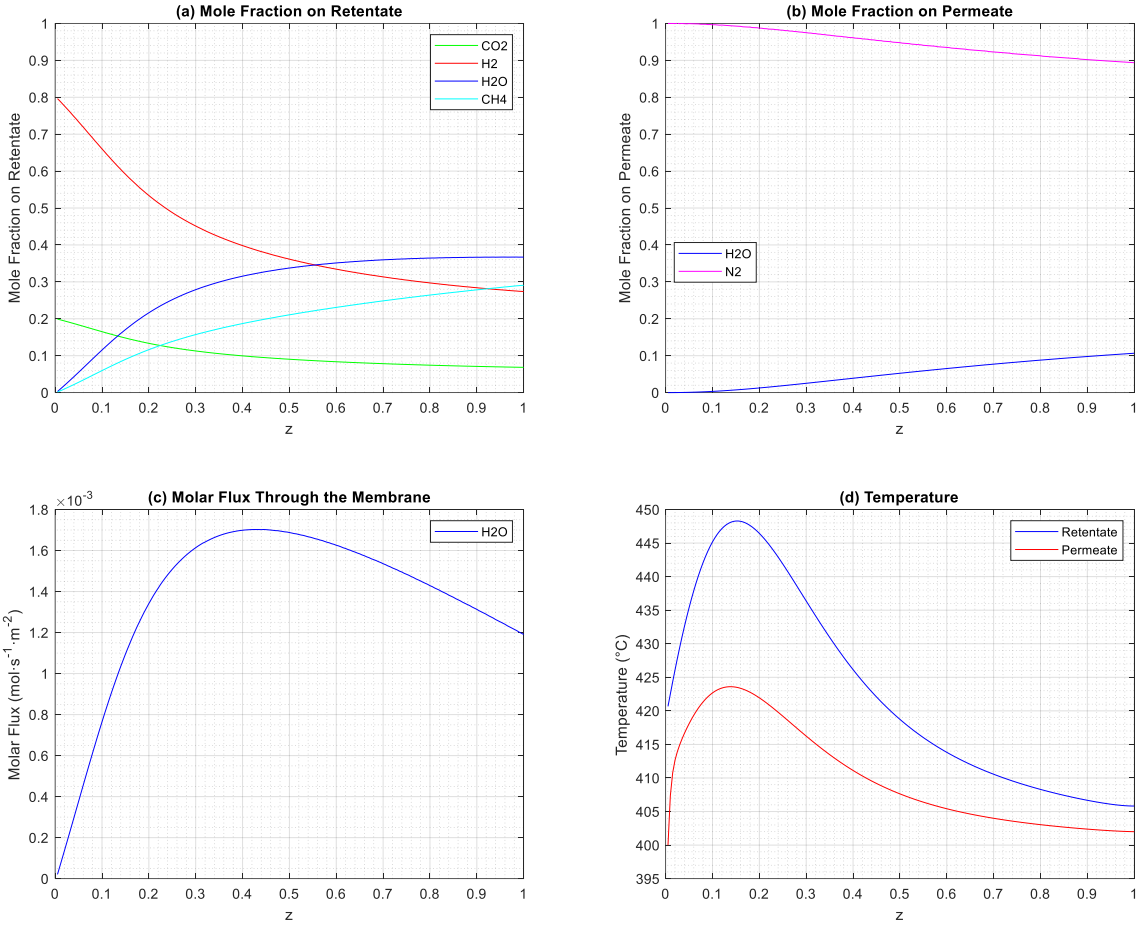

Figure 4-6. Data obtained for a Membrane Reactor with the characteristics presented in Table 4-1 and employing an ideal membrane, selective only towards steam. Feed streams with a space velocity of 20 $L_{STP} \cdot h^{-1} \cdot g_{cat}^{-1}$ and conditions of 395 °C and 1 atm (retentate) or 0.666 atm (permeate).

Since the permeate feed stream are not fed with CO_2 and there are no reactants lost through the membrane, the system conversion is equal to the catalytic bed conversion which is 80.9%, higher than the 74.6% presented by the traditional reactor. As a result, the hot spot for this case reached the highest value presented until now, about 448 °C, as shown in Figure 4-6(d). In Figure 4-6(a) is

possible to observe that the outlet stream of the retentate has a molar content of 30% methane (about 46% in dry basis, i.e. after removing all water by simple condensation) against the 21% in the traditional reactor (37% in dry basis), which is a significant improvement.

These results mean that with the membrane reactor it is possible to achieve higher conversions than in a traditional reactor, with higher concentrations of products with the same conditions of operation or the same quality of outlet streams under milder conditions. Unfortunately, these improvements rely on an ideal membrane (by now), which only permeates water (cf. Figure 4-6(b) and Figure 4-6(c)).

4.1.4 Membrane Reactor with Split Feed

Another alternative to prevent the loss of reactants through the membrane is to split the feed stream into two with equal molar flow rate, one for the retentate and one for the permeate (cf. Figure 3-3). Thus, the molar flux of such species (CO_2 and H_2) permeating from the retentate through membrane would be reduced due to a lower driving-force (because the partial pressure of CO_2 and H_2 on the retentate and permeate would be closer).

Indeed, it would be better if there was no need to use reactants to feed the permeate because a significant part does not pass through the catalytic bed (retentate zone), and the fraction which can permeate to the catalytic bed has a lower contact time when compared with reactants fed directly in the retentate.

However, this kind of configuration may be worth using if the permeate stream obtained is easily recyclable. It will depend however on the cost of recycling the reactants present in the permeate and the gap (i.e. improvement) between the catalyst bed conversion of a membrane reactor and the conversion of a traditional reactor fed axially with the same molar flow rate.

To test the improvements provided using reactants in permeate feed, a membrane reactor was simulated with the same dimensions and conditions as presented in Figure 4-4. The results are shown in Figure 4-7.

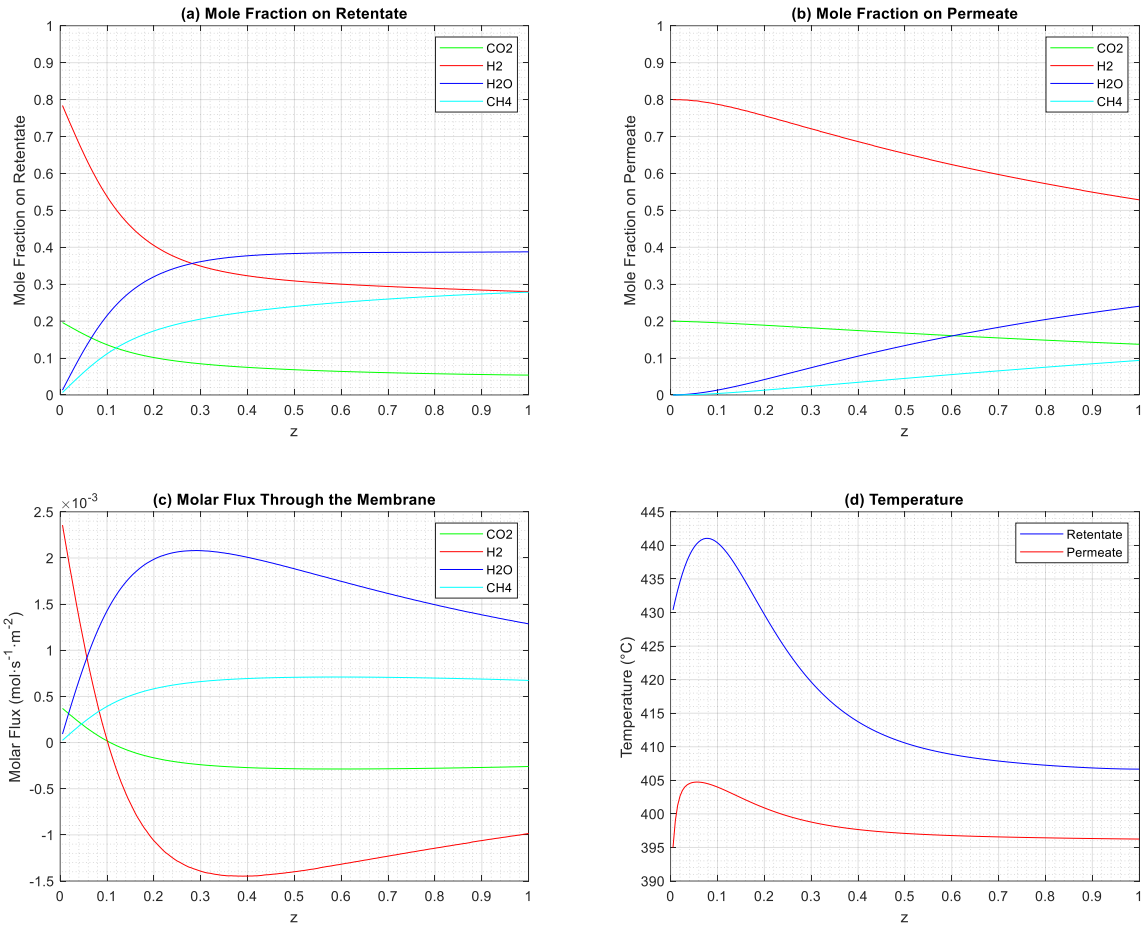

Figure 4-7. Data obtained for a Membrane Reactor with the characteristics presented in Table 4-1 but with the feed split 50/50 between retentate and permeate. Feed streams with a space velocity of 10 $L_{STP} \cdot h^{-1} \cdot g_{cat}^{-1}$ and conditions of 395 °C and 1 atm (retentate) or 0.666 atm (permeate).

Looking at the molar flux permeating through the membrane (cf. Figure 4-7(c)), it is possible to note that despite there is some loss of reactants in the first 10% of the reactor bed, afterwards the reactor bed starts to "pull" these reactants back again due to their consumption in the retentate (please notice the negative fluxes in such figure). In general, more reactants were entering the catalytic bed from the permeate than leaving the retentate, as observed in Figure 4-7(b).

Additionally, the membrane proved to be efficient in separating water from the retentate stream: 66% of all water produced permeated the membrane. If considering only the amount of CO_2 which entered the catalytic bed, either axially (fed in the retentate) or radially (permeated from the permeate to the retentate side), the CO_2 conversion amounts to 90.2% (herein called conversion of the catalytic bed, Eq. (3-32)), which is higher than the conversion of a traditional reactor (82.2%, data not shown) fed axially with the same amount of reactants that could reach the catalytic bed (axially or radially). Moreover, the catalytic bed conversion obtained is even higher than the CO_2 conversion of this traditional reactor in chemical equilibrium (84.7%, data not shown) at the same inlet conditions (395 °C and 1 atm).

However, this reactor configuration has two main problems. Firstly, only 18% of the CO_2 fed in the permeate stream passes through the catalytic bed, resulting in a system CO_2 conversion of 54% (Eq. 3-30), which is substantially lower than the 74.6% presented by a traditional reactor, which implies that for this reactor be economically viable, the recycling of reactants must be economically feasible so it is possible to take advantage of the high conversions in the catalytic bed (90.2%). Secondly, although it is economically reasonable to separate water from the reactants in the permeate, a considerable part of the methane produced (52%) also goes to the permeate. This makes the potential treatment of that stream for recycling the unconverted reactants leaving the permeate much more complex than just condensing water. Hence, this configuration is particularly recommended in the absence of methane in the permeate.

4.1.5 Traditional Reactor vs Membrane Reactor: Overview

Finally, simulations were performed to compare the performance of the traditional and membrane reactor considering different pressure ratio values. Additionally, they were also compared with a membrane reactor including an ideal membrane (as in Figure 4-6) for a pressure ratio of 0.666 and in the temperature range of 250 °C - 410 °C. The results are shown in Figure 4-8.

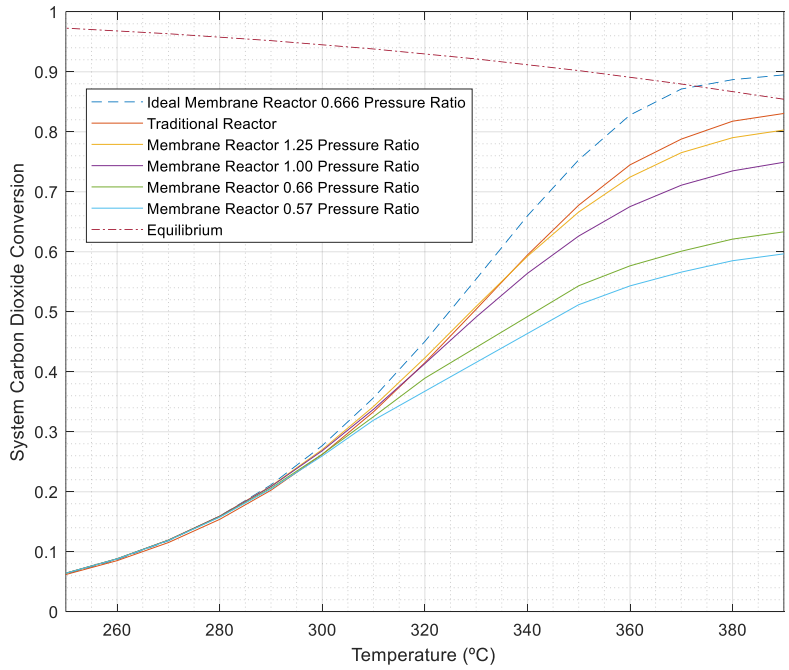

Figure 4-8. Comparison between the System CO_2 Conversion (Eq. 3-30) of Traditional Reactor and Membrane Reactor. The pressure on the retentate feed is 1 atm. All systems are fed with the same reactant molar flow rate, with a space velocity of 12 $L_{STP} \cdot h^{-1} \cdot g_{cat}^{-1}$. In the case of the Membrane Reactors without ideal membrane, the reactant molar flow rate is split equally: 6 $L_{STP} \cdot h^{-1} \cdot g_{cat}^{-1}$ for permeate and 6 $L_{STP} \cdot h^{-1} \cdot g_{cat}^{-1}$ for retentate. In the case of the Membrane Reactor with the ideal membrane, there is a reactant space velocity of 12 $L_{STP} \cdot h^{-1} \cdot g_{cat}^{-1}$ in retentate and 12 $L_{STP} \cdot h^{-1} \cdot g_{cat}^{-1}$ of N_2 in permeate, similar to Figure 4-6.

The ideal membrane reactor, which has the same characteristics as the one presented at Figure 4-6, proved to surpass the traditional reactor for the entire temperature range. Hence, either presents a higher conversion at the same operating conditions or the same conversion under milder conditions of temperature, showing the potential of the membrane reactor depending on the development of a new membrane with the desired characteristics.

Besides, looking at Figure 4-8 is possible to observe that decreasing the permeate feed pressure (and so pressure ratio) reduces the system CO_2 conversion since there are fewer moles of reactants that can enter the catalytic bed. Actually, increasing the pressure ratio makes the system increasingly resemble the traditional reactor, but always with a lower system conversion.

At this stage it is important to recall that, if the system conversion is lower than the traditional reactor, it does not necessarily mean that using a membrane reactor is worthless. As discussed previously, this index does not consider the advantages of the outlet streams being split in two. Unlike the traditional reactor, where all output products are mixed in one single stream, it is easier to recover (and recycle) the permeate stream if it is composed by reactants and water only, therefore needing to feed lower quantities of reactants and so relying on the high efficiency of the catalytic bed. That is why having a high catalytic bed CO_2 conversion is so important.

Finally, the loss of methane to the permeate could not be satisfactorily avoided in any simulation performed in this work. Thus, it is concluded that even avoiding the excessive loss of reactants by changing the permeate feed, the passage of CH_4 through the membrane severely undermines the greatest advantage of using a membrane reactor: to achieve a catalytic bed with superior conversion and, simultaneously, produce a permeate stream that can be easily recycled (i.e. without any product).

However, the high values of methane permeance are not found for methanol, as observed in Figure 3-2. Methanol permeance values are very close to zero in the temperature range presented, and so it has a higher potential to be explored, at least with this membrane, which will be discussed in the following section.

4.2 CO_2 Conversion Into Methanol

4.2.1 Kinetic Model Validation

The kinetic law for methanol production considered was based on the article by Portha, *et al.* (Portha, *et al.*, 2017). which proposes this model for two non-commercial catalysts, $Cu/ZnO/Al_2O_3$ and $Cu/ZnO/ZrO_2$, tested in a fixed-bed reactor whose characteristics are shown in Table 4-3.

Table 4-3. Characteristics of the reactor utilized to obtain the experimental data *(Portha, et al., 2017)*.

Length (cm)	0.382
Internal Diameter (mm)	10.1
Catalyst Particles Diameter (μm)	100
Catalyst Mass (mg)	135

A series of experiments were carried out by the authors in the interval described in Table 4-4 and the compounds in the output flow were analyzed by gas chromatography.

Table 4-4. Experimental conditions utilized to obtain the experimental data *(Portha, et al., 2017)*.

Temperature (°C)	200-230
Pressure (bar)	50-80
Space Velocity ($mL_{STP} \cdot h^{-1} \cdot g_{cat}^{-1}$)	17.72 – 53.16
H_2/CO_2 Inlet Ratio (mol_{H2}/mol_{CO2})	2-6

On that paper, the determination of the rate constants was accomplished considering an isothermal homogeneous plug-flow reactor model, and the kinetic law was suggested by the authors based on the model presented in other studies (Graaf, *et al.*, 1986; Graaf, *et al.*, 1988), with modification of the kinetic constants for reactions (2.1) and (2.2). The kinetic model and the respective kinetic, equilibrium, and adsorption constants suggested by Portha *et al*. (2017) for the $Cu/ZnO/Al_2O_3$ catalyst used in this work are shown below (Eq. 4-4):

$$\Re'_{2.1} = k_{2.1} \cdot b_{CO_2} \cdot \left\{ \frac{p_{CO_2} \cdot p_{H_2}^{3/2} - \frac{p_{CH_3OH} \cdot p_{H_2O}}{p_{H_2}^{3/2} \cdot K_{2.1}}}{\left(1 + b_{CO} \cdot p_{CO} + b_{CO_2} \cdot p_{CO_2}\right) \cdot \left[p_{H_2}^{1/2} + \left(\frac{b_{H_2O}}{b_{H_2}^{1/2}} \right) \cdot p_{H_2O} \right]} \right\} \quad \text{Eq. 4-4}$$

$$\Re'_{2.2} = k_{2.2} \cdot b_{CO_2} \cdot \left\{ \frac{p_{CO_2} \cdot p_{H_2} - \frac{p_{CO} \cdot p_{H_2O}}{K_{2.2}}}{\left(1 + b_{CO} \cdot p_{CO} + b_{CO_2} \cdot p_{CO_2}\right) \cdot \left[p_{H_2}^{1/2} + \left(\frac{b_{H_2O}}{b_{H_2}^{1/2}} \right) \cdot p_{H_2O} \right]} \right\} \quad \text{Eq. 4-5}$$

$$\Re'_{2.3} = k_{2.3} \cdot b_{CO} \cdot \left\{ \frac{p_{CO} \cdot p_{H_2}^{3/2} - \frac{p_{CH_3OH}}{p_{H_2}^{1/2} \cdot K_{2.3}}}{\left(1 + b_{CO} \cdot p_{CO} + b_{CO_2} \cdot p_{CO_2}\right) \cdot \left[p_{H_2}^{1/2} + \left(\frac{b_{H_2O}}{b_{H_2}^{1/2}} \right) \cdot p_{H_2O} \right]} \right\} \quad \text{Eq. 4-6}$$

$$\log_{10}(K_{2.1}) = \frac{3066}{T} - 10.592 \quad \text{Eq. 4-7}$$

$$\log_{10}(K_{2.2}) = \frac{-2073}{T} - 2.029 \quad \text{Eq. 4-8}$$

$$\log_{10}(K_{2.3}) = \frac{5139}{T} - 12.621 \qquad \text{Eq. 4-9}$$

$$b_{CO} = 2.16 \cdot 10^{-5} \cdot \exp\left(\frac{46800}{R \cdot T}\right) \qquad \text{Eq. 4-10}$$

$$b_{CO_2} = 7.05 \cdot 10^{-7} \cdot \exp\left(\frac{61700}{R \cdot T}\right) \qquad \text{Eq. 4-11}$$

$$\frac{b_{H_2O}}{b_{H_2}^{1/2}} = 6.37 \cdot 10^{-9} \cdot \exp\left(\frac{84000}{R \cdot T}\right) \qquad \text{Eq. 4-12}$$

$$k_{2.1} = 23.4 \cdot \exp\left(\frac{-52570}{R \cdot T}\right) \qquad \text{Eq. 4-13}$$

$$k_{2.2} = 4.84 \cdot 10^{11} \cdot \exp\left(\frac{-140020}{R \cdot T}\right) \qquad \text{Eq. 4-14}$$

$$k_{2.3} = 4.89 \cdot 10^{7} \cdot \exp\left(\frac{-113000}{R \cdot T}\right) \qquad \text{Eq. 4-15}$$

Using the kinetics suggested for the $Cu/ZnO/Al_2O_3$ catalyst determined by Portha *et al.* (2017), simulations were performed in the computational model developed in the framework of the present work trying to replicate the experimental results on the original paper, carried out between 200 °C and 230 °C, at 50 bar and with a volumetric flow rate of 30.49 $mL_{STP} \cdot min^{-1}$. The molar contents of the feed stream were 17.8% CO_2, 69.8% H_2 and 12.4% N_2. The simulated reactor had the same characteristics as reported in the original paper (*cf.* Table 4-3).

The H_2 conversion was determined and compared with those obtained experimentally by Portha *et al.* (2017), and the results are shown in Figure 4-9.

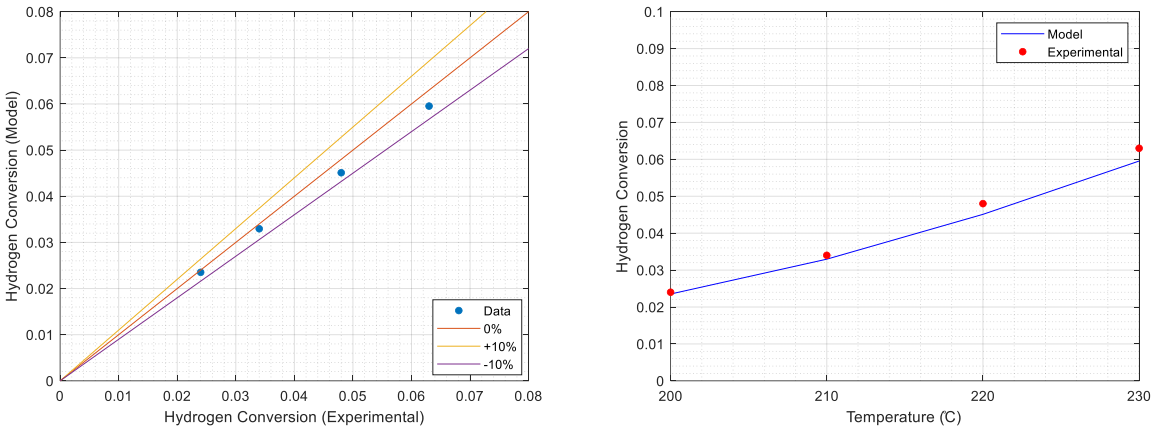

Figure 4-9. Comparison between the data obtained through the model used in this work and the experimental data collected from the literature (Portha, *et al.*, 2017). (a) Parity plot; (b) Hydrogen Conversion;

The results demonstrate that the computational model developed in this work presents conversions systematically slightly lower than those observed experimentally in the original paper.

This can be related to the fact that the determination of constants was performed in a model without axial dispersion. Even so, predictions were considered satisfactory since no error greater than 6% was observed.

4.2.2 Traditional Reactor: Overview

Next, a traditional reactor with the characteristics pointed in Table 4-5 was simulated.

Table 4-5. Characteristics of the theoretical reactor utilized for the methanol simulations in this work.

Length (cm)	3.82
Internal Diameter (mm)	10.1
Catalyst Particles Diameter (µm)	100
Catalyst Mass (mg)	1350

The operating conditions chosen were 270 °C and 50 atm because they are commonly used in the production of methanol (Palma, *et al.*, 2018). The molar content of the feed stream considered was 25% CO_2 and 75% H_2, based on the H_2/CO_2 stoichiometric ratio of 3. The concentration, temperature, and molar flow rate profiles are shown in Figure 4-10.

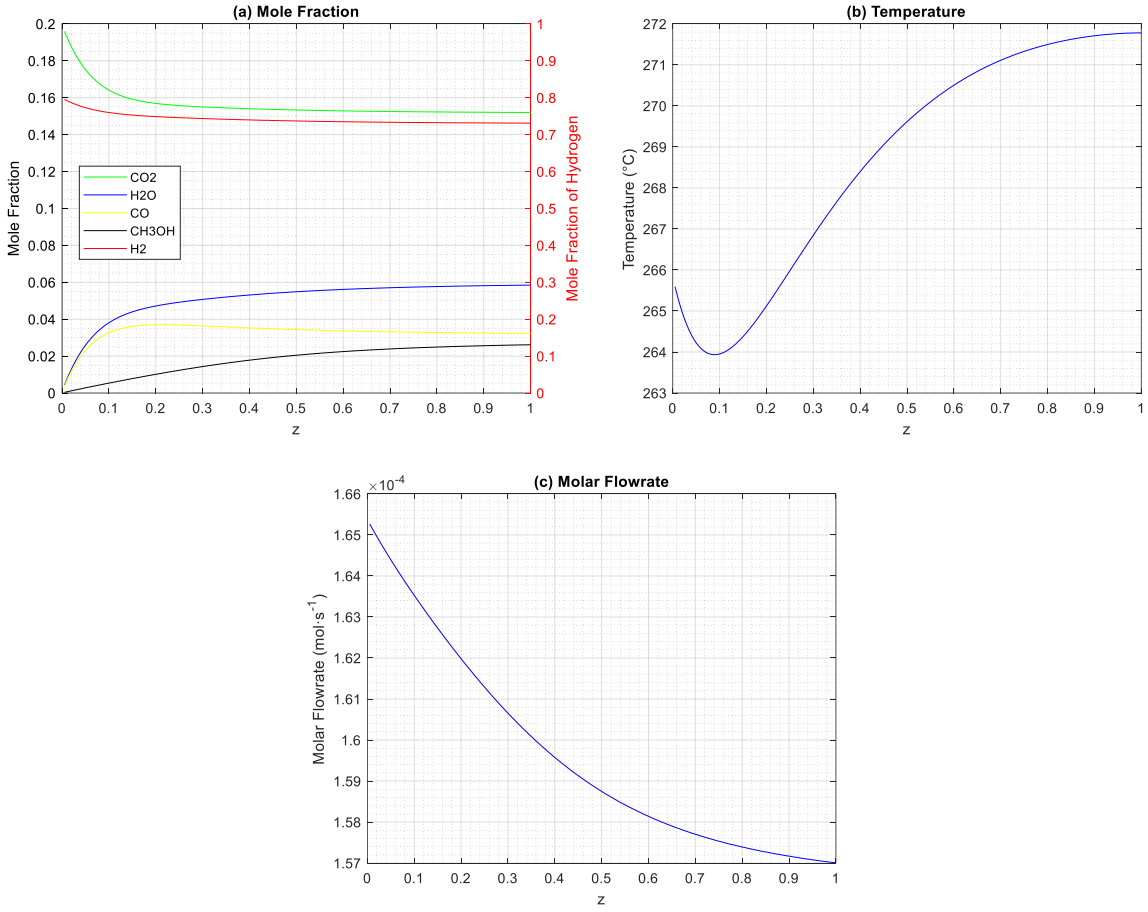

Figure 4-10. Data obtained for a Traditional Reactor with the characteristics presented in Table 4-5. Feed stream conditions of 270 °C and 50 atm with a space velocity of 12 $L_{STP} \cdot h^{-1} \cdot g_{cat}^{-1}$.

Similarly to section 4.1.2 this case-study will serve not only to observe the most important characteristics related to methanol production but also as a benchmark to compare all membrane reactor configurations proposed herein to produce methanol. Since it is a traditional reactor, the system conversion and the conversion of the catalytic bed are equal and presents a value of 23.41%.

One difference regarding methane production is the temperature profile. For methanol production there is some cooling at the beginning of the reactor before the reactor bed warms up. It occurs because the formation of CO and CH_3OH does not happen at the same ratio through the reactor. This difference between carbon monoxide and methanol production rate can be observed in Figure 4-10(a). So, since the production of CO (Eq. 2-2) is endothermic, it generates a decrease of temperature at the start of the reactor (where the highest amount of CO is produced). However, this increases the concentration of CO and leads to the equilibrium of that reaction. On the other hand, despite the production of CH_3OH (Eq. 2-1, exothermic) does not have the same initial reaction rate as Eq. 2-2 and takes more contact time to reach its equilibrium, after a certain point the heat produced by Reaction 2.1 surpasses the heat consumed by Eq. 2-2. Besides, part of the CO produced is converted to CH_3OH as well, through Eq. 2-3, releasing even more heat.

Figure 4-10(b) shows the temperature curve starting at approximately 265.5 °C for z=0, despite the feed temperature being 270 °C. That difference occurs due to the Danckwert's boundary conditions. For the methanol case, such discontinuity reduces the temperature of the first point as the production of CO is endothermal.

In order to study the dependencies of the feed temperature and pressure, a series of simulations were made in the interval between 150 °C and 310 °C, from 10 atm to 70 atm, comparing the performance of the traditional reactor with the equilibrium conversion (calculated based on feed conditions). The results are shown in Figure 4-11.

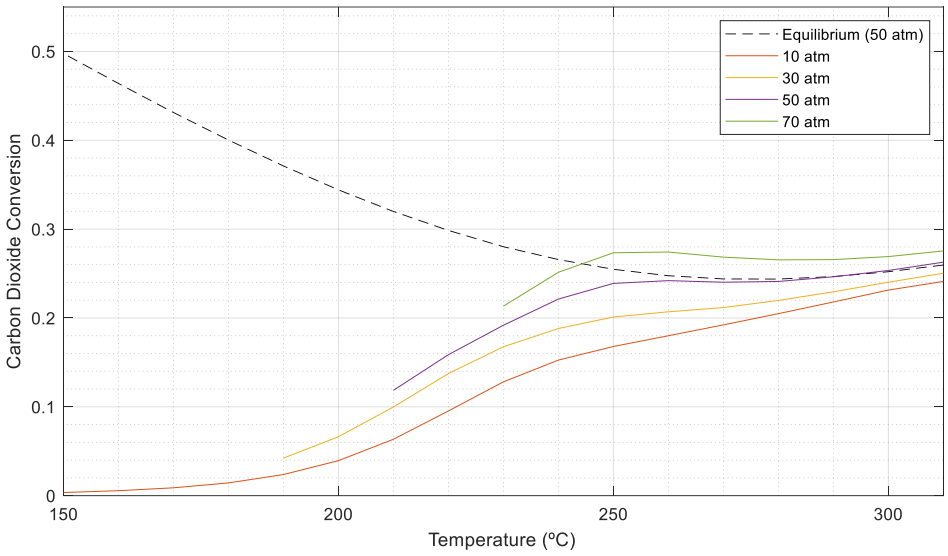

Figure 4-11. X_{CO_2} obtained with a Traditional Reactor for different conditions of temperature and pressure on the feed stream. The reactor characteristics are presented in Table 4-5. A space velocity of 5 $L_{STP} \cdot h^{-1} \cdot g_{cat}^{-1}$ was considered for all simulations. Continuous lines are model predictions while dashed line refer to equilibrium conversion.

Figure 4-11 shows that, at milder conditions, the reaction is limited by the kinetics and so increasing either the temperature or the pressure will lead to higher CO_2 conversions, similarly to the case of methane.

The increase of pressure shifts the equilibrium to higher conversions of CO_2 since both Eq. 2-1 and 2-3 take place with a decrease of the number of moles, although the pressure should not influence Eq. 2-2 from the thermodynamic point of view). However, the same does not happen with the change of temperature: at lower values, its increasing spoils CO_2 equilibrium conversion since the methanol production is exothermal – please note the dashed-dot lines in Figure 4-11. However, it is worth mentioning that the production of carbon monoxide is endothermic (cf. Eq. 2-2). Therefore, for higher temperatures, the decrease of CO_2 equilibrium conversion by shifting Eq. 2-1 and 2-3 does not compensate the increase by shifting Eq. 2-2, and then the CO_2 equilibrium conversion increases with an increase in temperature.

With that in mind, a higher CO_2 conversion, for methanol production, does not necessarily mean better performance: higher temperatures will impair the selectivity towards methanol in this system of reactions, producing CO instead of CH_3OH. For this reason, for all the subsequent cases, the analysis will focus on methanol yield instead of CO_2 conversion, defined as the amount of methanol produced over the amount of CO_2 fed to the system (Eq. 3-31) or to the bed (Eq. 3-33).

4.2.3 Membrane Reactor with Split Feed

A membrane reactor was used to improve the yield of CH_3OH by shifting the equilibrium through water removal. As discussed previously, the use of N_2 in the permeate feed is not worth considering since the extrapolated membrane permeances at the considered operating temperatures

results in the considerable loss of reactants (CO_2 and H_2). So, the feed stream was split in two equal streams, one fed to the permeate and the other to the retentate, similar to what was done in Figure 4-7. The pressure ratio chosen was 1. All other input variables remained the same. The results are shown in Figure 4-12.

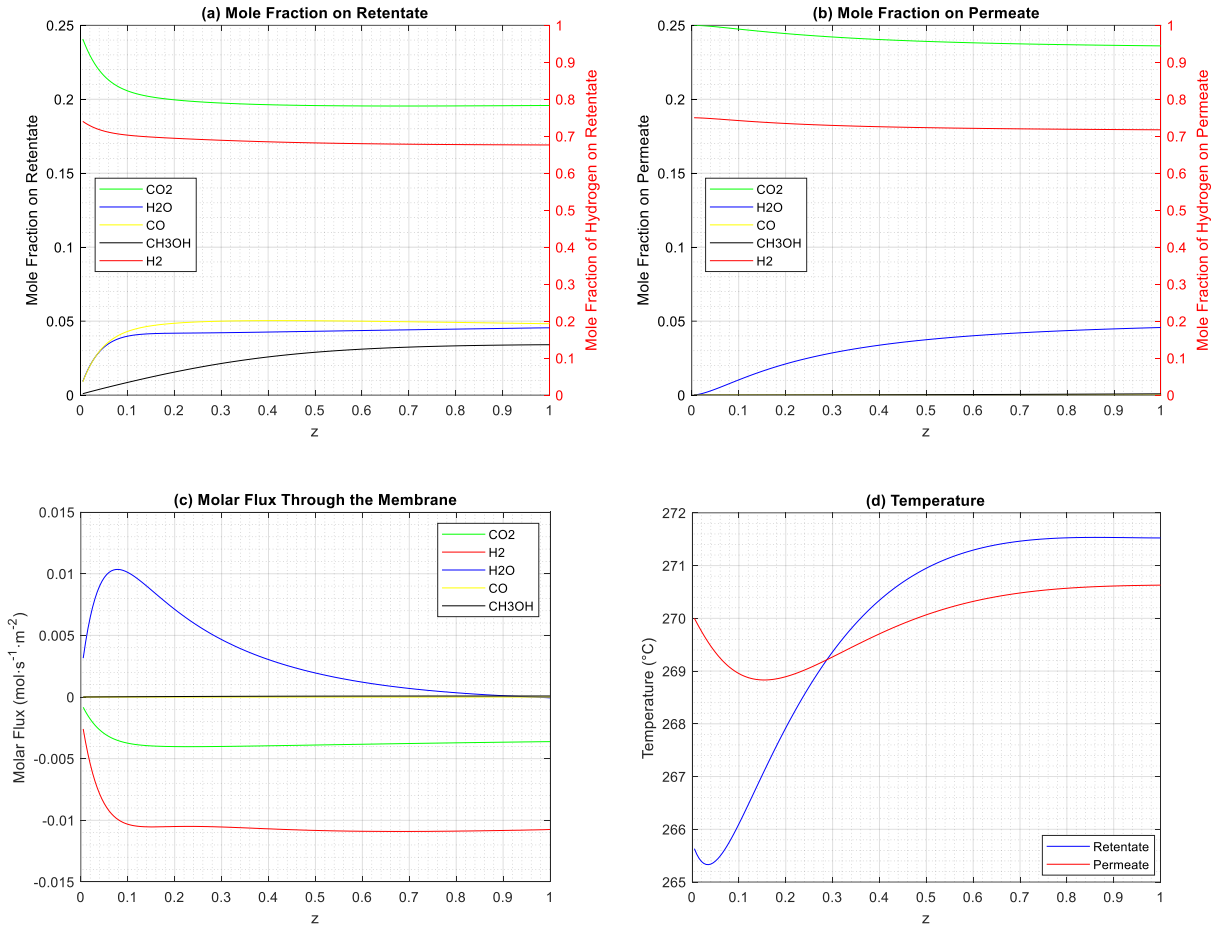

Figure 4-12. Data obtained for a Membrane Reactor with the characteristics presented in Table 4-5 but with split of the feed into the retentate and permeate. Feed streams with a space velocity of 6 $L_{STP} \cdot h^{-1} \cdot g_{cat}^{-1}$ each and conditions of 270 °C and 50 atm.

Based on the data from Figure 4-12(a) and Figure 4-12(b) and inherent flow rates, the system methanol yield is 7.35%, which represents a value 20% lower than the 9.12% obtained with the traditional reactor presented in Figure 4-10. But, as explained previously, it just indicates that this unit alone is less efficient to produce methanol and this index does not consider that a significant part of the reactant fed passes through the permeate without contacting the catalyst and can be recycled more easily than it would be if mixed with methanol in the retentate.

It is possible to observe in Figure 4-12(c) that water is the only compound that has entered the permeate significantly (positive flux). In fact, 45% of all water produced in the catalytic bed was removed through the permeate. Furthermore, a significant part of the reactants on the retentate entered the catalytic bed coming from the permeate chamber: 14.65% of all moles of reactants fed to

the bed did it by radial feed, contributing to the maintenance of their concentration in the retentate side (Figure 4-12.(a)) and its reduction in the permeate (Figure 4-12(b)).

The membrane reactor presented a catalytic bed methanol yield of 12.46%, which represents a value 22% higher than the 10.23% presented by a traditional reactor fed axially with the same molar flow rate that entered the catalytic bed (data not shown). This is a satisfactory result since it presents a higher methanol yield than its equivalent traditional reactor and so the membrane reactor has the potential to surpass the traditional reactor through the recycle of reactants present on the exit permeate stream, if not contaminated or easily purified.

Nevertheless, decreasing the total pressure on the permeate side (and so decreasing the pressure ratio) can potentially improve water removal (due to a higher permeation driving force) and so improve the catalytic bed CO_2 conversion. Considering that, a reactor with the same conditions as the one in Figure 4-12, but with a pressure ratio of 2/3, was simulated. The results are shown in Figure 4-13.

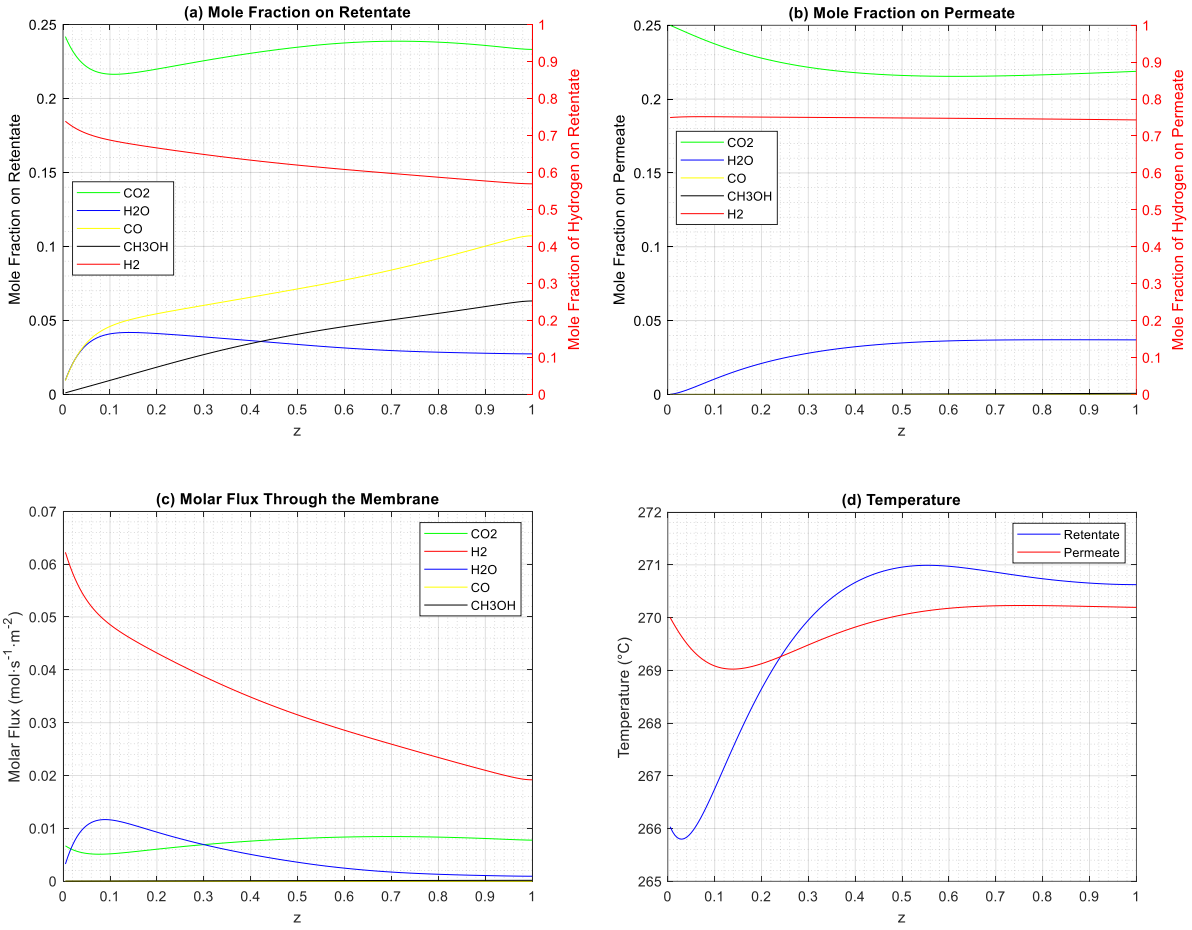

Figure 4-13. Data obtained for a Membrane Reactor with the characteristics presented in Table 4-5. Both feed streams (retentate and permeate) with a space velocity of 6 $L_{STP} \cdot h^{-1} \cdot g_{cat}^{-1}$ and conditions of 270 °C and 50.00 atm (retentate) or 33.33 atm (permeate).

Decreasing the pressure ratio, the system yield of methane dropped from 7.35% to 5.21%, which is considerably lower than the 9.12% presented by the traditional reactor. This was expected since now there is no radial feed of reactants to the catalytic bed, as observed in Figure 4-13(c). This decrease in the reaction extent can be observed by comparing the temperature profiles of Figure 4-12(d) and Figure 4-13(d), which has a slightly lower amplitude.

However, there was also a decrease in the bed yield of methane: from 12.46% to 10.42%. This indicates that the decrease in the permeate pressure, despite promoting the passage of water (which would shift the equilibrium forward and increase the yield of the catalytic bed) did not compensate for the loss of reactants that in turn will not react and negatively influence the CH_3OH yield of the bed.

4.2.4 Traditional Reactor vs Membrane Reactor: Overview

In order to study the influence of the permeate feed pressure in the **methanol yield of the system**, numerous simulations were made in a temperature range between 210 °C and 310 °C for different values of pressure ratio and the results were compared with a traditional reactor and a membrane reactor with an ideal membrane. The results are shown in Figure 4-14.

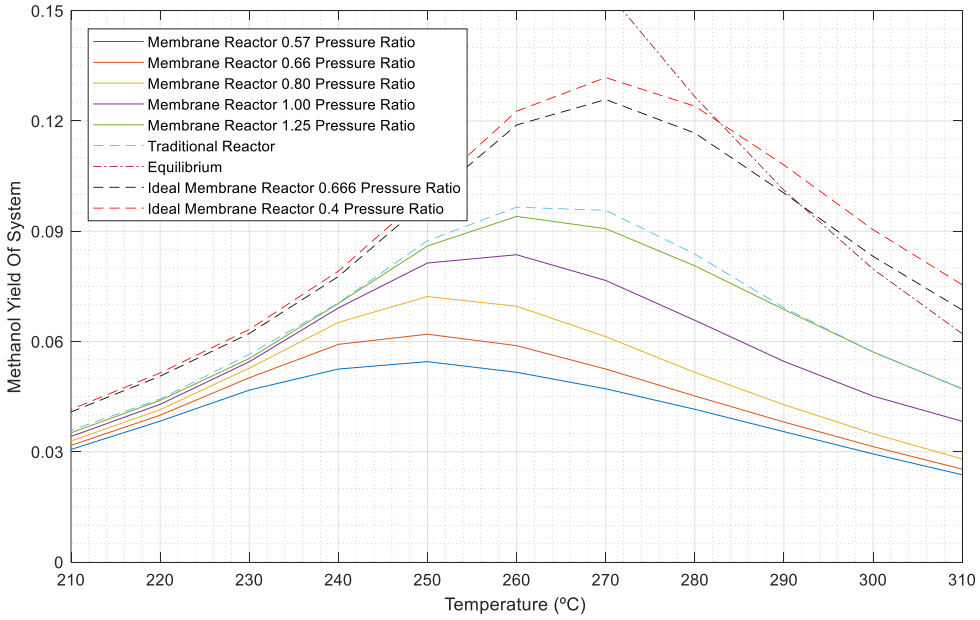

Figure 4-14. Comparison between Traditional Reactor and Membrane Reactor. The pressure on the retentate feed is 50 atm. All systems are fed with the same reactant molar flow rate, with a space velocity of 10 $L_{STP} \cdot h^{-1} \cdot g_{cat}^{-1}$. In the case of a Membrane Reactor with the ideal membrane, there is also a feed flow rate of 10 $L_{STP} \cdot h^{-1} \cdot g_{cat}^{-1}$ of N_2 in the permeate. In the case of all others Membrane Reactors, its feed is split equally between the retentate and permeate (space velocity of 5 $L_{STP} \cdot h^{-1} \cdot g_{cat}^{-1}$ each).

First, differently of the CO_2 conversion into methane which presents approximately constants or even increasing values for higher temperatures, the yield of CH_3OH reaches a maximum before it

starts to decrease with the increase of temperature since the selectivity of CH_3OH over CO starts to decrease.

In Figure 4-14 is possible to observe that the lower the pressure ratio, the lower is the amount of methanol produced and so a lower methanol yield of the system is obtained. This happens because there is a smaller amount of reactants entering the catalytic bed and, in some cases, the catalytic bed (retentate) may even lose reactants to the permeate side.

However, for higher pressure ratios, the system will resemble a traditional reactor: progressively higher amounts of reactants are forced to pass through the bed, and lower amounts of water are permeating the membrane. Yet, it never surpasses a traditional reactor since, in addition to always remaining some amount of reactants in the permeate, radial feed presents a lower contact time with the catalyst than axial feed, not compensated by water permeation fluxes that are becoming smaller when the permeate pressure increases.

Also, since the ideal membrane allows all reactants to be fed axially into the catalytic bed, it presents the highest amount of methanol produced due to the highest contact time of the methanol fed into the whole system. Indeed, the membrane reactor with the ideal membrane outperformed not only the traditional reactor but also the chemical equilibrium, for some temperatures. Besides, as all reactants are fed to the retentate, the methanol yield of the system is equal to the methanol yield of the catalytic bed for the same flow rate.

Then, to study the influence of the permeate feed pressure in the **methanol yield of the catalytic bed**, simulations were made in an interval between 210 °C and 310 °C for different values of pressure ratio and the results were compared with a traditional reactor and a membrane reactor with an ideal membrane. The results are shown in Figure 4-15.

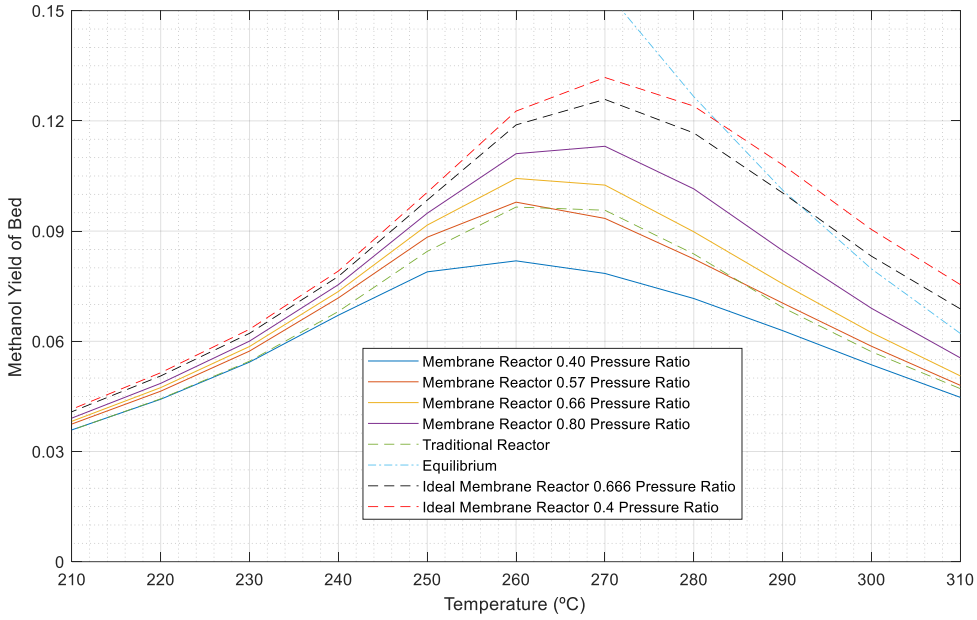

Figure 4-15. Comparison between Traditional Reactor and Membrane Reactor. The pressure on the retentate feed is 50 atm. All beds are fed with the same reactant molar flow rate, with a space velocity of 10 $L_{STP} \cdot h^{-1} \cdot g_{cat}^{-1}$. In the case of a Membrane Reactor with the fictional membrane, there is also a feed flow rate of 10 $L_{STP} \cdot h^{-1} \cdot g_{cat}^{-1}$ of N_2 in the permeate. In the case of all others Membrane Reactors, its feed is split equally between the retentate and permeate (space velocity of 10 $L_{STP} \cdot h^{-1} \cdot g_{cat}^{-1}$ each).

According to Figure 4-15, for the four pressure ratios simulated, there are two which outperformed the traditional reactor in terms of methanol yield of the bed (pressure ratio of 0.80 and 0.66), one which performed similarly to a traditional reactor (0.57), and one which performed worse than the traditional reactor (0.40). It happened because if the pressure on the permeate is much smaller than in the retentate, there is a high amount of reactants being lost before they could react in the catalytic bed, reducing the amount of methanol produced. This illustrates, in a wide range of temperatures, the behavior observed in Figure 4-13: the increase of water permeated due to a decrease in pressure ratio does not compensate for the loss of reactants, and so higher pressure ratios lead, to some extent, to higher catalyst bed yields of methanol.

On the other hand, if the pressure on the permeate is too high (data not shown)[2], it will decrease the amount of water permeating the membrane, although a significant part of the feed on the catalytic bed will occur radially and, as mentioned before, despite it increases the amount of product generated on the catalytic bed (and so the methanol yield of the system) it decreases the methanol yield of the bed since feeding radially implies a lower contact time with the catalyst than

[2] These cases are not illustrated because every case of membrane reactor would have a different amount of reactants fed radially and so each point would need a traditional reactor fed with a different reactant stream.

axially, reducing the amount of methanol produced per carbon dioxide fed. This effect is also observed in Quench Reactors, mentioned in the State of the Art.

So, the pressure ratio which leads to the highest methanol yield of the bed is the one which is high enough to block the reactant loss from the retentate through the membrane, but yet low enough to avoid radial feed from the permeate. However, since the flux through the membrane is variable throughout the reactor and different for each component, there is always a driving force (different partial pressures) and this scenario only happens in membranes that has the permeance of reactants equal to zero: this is the case of the reactor with the fictional membrane which represents the highest improvement in the efficiency of the catalytic bed since no reactants were permeating the membrane (neither as a loss nor as an inefficient radial feed).

In this case, the greater the pressure difference between the permeate and the retentate, the greater the methanol yield since it will increase the amount of water permeating without losing any reactants.

4.2.5 The Global Yield of Methanol

So far, the use of membranes to improve the effectiveness of a catalytic bed has been studied and evaluated for methane and methanol. But one question remains: is this the most important index to be taken into account when deciding the feasibility of the process?

Despite the radial loss of reactants implies a lower catalytic bed yield of methanol, once the stream that leaves the catalytic bed radially goes to a permeate stream which is substantially easier to be recovered, some decisions are placed on the agenda.

For example, in the case presented in Figure 4-13, it was seen that with the reduction of the pressure ratio there was a decrease of methanol yield in the catalytic bed due to the great loss of reactants, which when transferred to the permeate ended up leaving the system without reacting. Considering that the permeate is composed practically by reactants and water vapor (the highest methanol molar fraction found was 0.005) and therefore is easily recyclable by simple condensation, this recycling implies a lower amount of reactants needed to feed the system. Therefore, it was decide to check whether it would be worth losing this bed efficiency if one could lower the overall need of reactants. In other words, it was decide to check whether the decrease of methanol produced could be compensated by the decrease of H_2 and CO_2 fed.

Considering this and the concept of Global Yield of Methanol (see section 3.4), the simulations carried out in Figure 4-15 were reassessed, but now the data obtained from the membrane reactor was compared with a traditional reactor (and a membrane reactor with the fictitious membrane) fed by the same amount of reactants needed to add to the recycle stream. The results are shown in Figure 4-16.

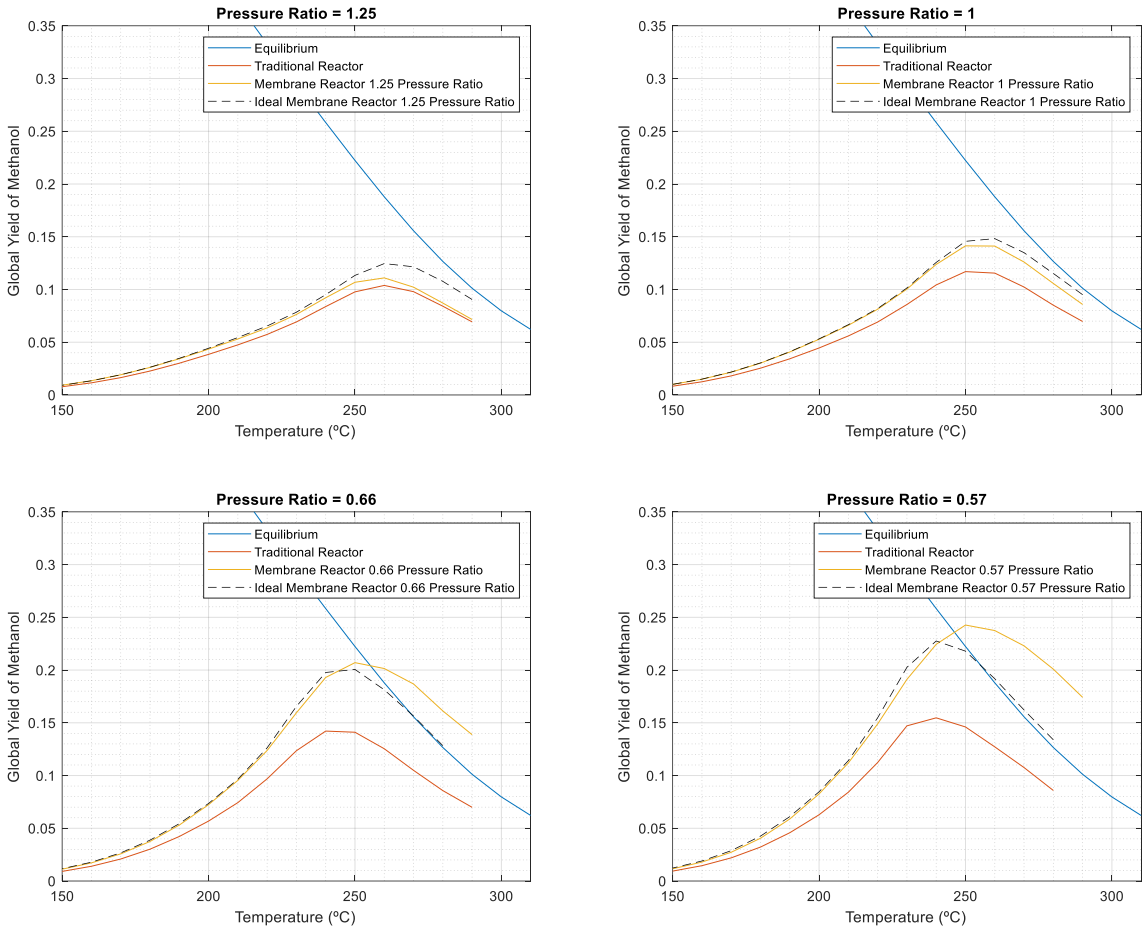

Figure 4-16. Comparison of the Global Yield of Methanol between Traditional Reactor and Membrane Reactor for different Pressure Ratios. For each case, the amount of reactant recycled was different and so the inlet streams for each case were settled to keep the system feed constant and with a space velocity of 10 $L_{STP} \cdot h^{-1} \cdot g_{cat}^{-1}$.

Looking at Figure 4-16, it is possible to notice that for a membrane reactor, in general, the lower the pressure of the permeate relative to the retentate (lower pressure ratio), the greater the global yield of methanol. This is because the index considers that any reactant that ends up in the permeate is 'de-feeding' the reactor so if all the H_2/CO_2 that has not reacted ends in the permeate, the global yield of methanol will be 1, even if there is very little production of methanol in the system.

Another fact to be noted is that with the decrease of pressure ratio it is possible not only to exceed the chemical equilibrium but also the fictitious membrane that permeates exclusively water, producing more methanol from the same amount of reactants. This indicates that, with the use of reactant recycling in the permeate stream, the fact that the membrane permeates reactants may even help the efficiency of the methanol production (relatively to the amount of reactants fed). This happens because, in order to increase the total number of converted molecules, it is more advantageous a molecule of CO_2/H_2 at any point along the reactor be recycled (and took back to the start) than remaining in the retentate stream.

For this reason, lowering the pressure ratio causes the yield of methanol to approach 1, removing all reactants that were not transformed into methanol from the catalytic bed to the

permeate. Therefore, the retentate stream flow rate will be smaller and smaller, with increasing concentrations of methanol since its permeance is much lower than every other compound.

However, this strategy cannot be used indiscriminately. It leads to the production of even smaller quantities of methanol that, even though the demand for reactants was proportionally small, there would be a need to treat and recycle an increasing stream of permeate and therefore increasing this source of operational cost.

In order to know the minimum amount of pressure ratio (if any) that would lead to a higher global methanol yield with a worth increase of operational cost treating the permeate stream, an economic analysis would be required, considering also the cost of treatment of the retentate stream. Such analysis was not carried out because was out of the scope of this work and remains as a suggestion for an interesting future work.

5 Conclusion and Suggestions for Future Work

In this work, a MATLAB program developed at LEPABE was adapted to simulate any gas phase catalytic reaction occurring inside a traditional or membrane tubular reactor, such as the hydrogenation of CO_2 into methane and methanol, whose predictions were validated against data available from the literature.

Several simulations were made, in an interval between 250 °C - 410 °C and 1 atm – 7 atm for methane and 150 °C - 310 °C and 10 atm – 70 atm for methanol production. The influence of intensive variables such as the feed temperature, pressure, and the ratio between the retentate and permeate pressure for membrane reactors was extensively discussed.

For methane, since its chemical equilibrium already allows reaching high conversions, the main goal of using a membrane reactor is to achieve these results under milder conditions of temperature and pressure (as compared to a traditional reactor), and so decrease the operational cost of the process. However, since the simulated hydrophilic SOD membrane (with properties taken from literature) has high values of permeance for H_2, CO_2, and CH_4, the permeate stream would also need to be fed with the two reactants to avoid their loss from the catalytic bed to the permeate side; still, since CH_4 permeates the membrane, the permeate outlet stream would also contain methane, and so this membrane reactor configuration is not justified, at least with this membrane, since the same streams fed in a traditional reactor would lead to a better result.

With an ideal membrane, set to ideally permeate only water, a feed stream at 360 °C was able to reach the same CO_2 conversion obtained with a traditional reactor fed at 410 °C. Moreover, at higher temperatures, the membrane reactor surpassed the chemical equilibrium. It shows the high potential of membrane reactors to improve chemical processes depending on the development of the materials science field, as well as the relevance of simulation work to establish reliable targets for materials improvement.

For methanol, the main goal of using a membrane reactor is to increase the methanol yield, very limited by the chemical equilibrium, and selectivity. In this case, the SOD membrane presents very low values of permeance for CH_3OH and so the use of a membrane reactor is more suitable. In fact, the methanol yield of the catalytic bed increased up to 18% using a membrane reactor, while a permeate outlet stream containing only reactants and water, and so easily recyclable, was obtained.

In order to know if this increase in production is worth considering, an economical study would be necessary, accounting for the treatment cost of the recycling stream and the capital cost of the membrane reactor, which would be an interesting future work.

6 References

Bagher, A. M., Vahid, M., Mohsen, M. & Parvin, D., 2015. Hydroeletric Advantages and Disadvantages. *American Journal of Energy Science,* Volume 2, pp. 17-20.

Blanco, H., Nijs, W., Ruf, J. & Faaij, A., 2018. Potential for hydrogen and Power-to-Liquid in a low-carbon EU energy. *Applied Energy*, Volume 232, pp. 617-639.

Court, V. & Fizaine, F., 2017. Long-Term Estimates of the Energy-Return-on-Investment (EROI) of. *Ecological Economics,* Volume 138, pp. 145-159.

Davidson, T., 1993. *Simple and accurate method for calculating viscosity of gaseous mixtures,* s.l.: Bureau of Mines.

Dolci, F., Thomas, D., Hilliard, S., Guerra, C. F., Hancke, R., Ito, H., Jegoux, M., Kreeft, G., Leaver, J., Newborough, M., Proost, J., Robinius, M., Weidner, E., Mansilla, C., Lucchese, P., 2019. Incentives and legal barriers for power-to-hydrogen pathways: An international snapshot. *International Journal of Hydrogen Energy,* 44(23), pp. 11394-11401.

Falbo, L., Martinelli, M., Visconti, C. G., Lietti, L., Bassano, C., Deiana, P., 2018. Kinetics of CO2 methanation on a Ru-based catalyst at process conditions relevant for Power-to-Gas applications. *Applied Catalysis B: Environmental*, Volume 225, pp. 354-363.

Faria, A. C., Miguel, C. V. & Madeira, L. M., 2019. *Modeling and simulation of a CO2 methanation membrane reactor.* Eindhoven: s.n.

Fichtl, M. B., Schlereth, D., Jacobsen, N., Kasatkin, I., Schumann, J., Behrens, M., Hinrichsen, O., Schlogl, R., 2015. Kinetics of deactivation on Cu/ZnO/Al2O3 methanol synthesis catalysis. *Applied Catalysis*, Volume 502, pp. 262-270.

Fiedler, E., Grossman, G., Kersebohm, D., Weiss, B., Witte, C., 2012. Methanol. Ullmann's Encyclopedia of Industrial Chemistry.

Gonçalves, R. V., 2011. *Dissertação: Projeto auxiliado por computador de processos indústriais sustentáveis usando os softwares COCO e Scilab,* Uberlândia: s.n.

Gotz, M., Lefebvre, J., Mors, F., Koch, A. M., Graf, F., Bajohr, S., Reimert, R., Kolb, T., 2016. Renewable Power-to-Gas: A technological and economic review. *Renewable Energy*, Volume 85, pp. 1371-1390.

Graaf, G. H., Sijtsema, P. J. J. M., Stamhuis, E. J. & Joosten, G. E. H., 1986. Chemical Equilibria in Methanol Synthesis. *Chemical Engineering Science*, 41(11), pp. 2883-2890.

Graaf, G. H., Stamhuis, E. J. & Beenackers, A. A. C. M., 1988. Kinetics of Low-Pressure Methanol Synthesis. *Chemical Engineering Science*, 43(12), pp. 3185-3195.

Griffiths, G. W., 1984. Optimize large methanol plants. *Hydrocarbon Processing*, Volume 63, pp. 95-100.

Harari, Y. N., 2019. *Sapiens: Breve História da Humanidade.* 20 ed. Amadora: Elsinore.

Hausfather, Z., 2017. *Carbon Brief.* [Online] Available at: https://www.carbonbrief.org/analysis-why-scientists-think-100-of-global-warming-is-due-to-humans
[Accessed on 08 March 2020].

Johansson, S., 2013. Limits to Biofuels. *EPJ Web of Conferences,* 54(01014).

Khademi, M. H. & Sabbaghi, R. S., 2017. Comparison between three types of ammonia synthesis reactor configurations in terms of cooling methods. *Chemical Engineering Research and Design*, Volume 128, pp. 306-317.

Kierzenka, J., 2016. *Matlab Central File Exchange.* [Online] Available at: Tutorial on solving BVPs with BVP4C (https://www.mathworks.com/matlabcentral/fileexchange/3819-tutorial-on-solving-bvps-with-bvp4c)

Lacis, A. A., Schmidt, G. A., Rind, D. & Ruedy, R. A., 2010. Atmospheric CO2: Principal Control Knob Governing Earth's Temperature. *Science,* 330(356), pp. 256-259.

Lackner, K. S., 2009. Capture of carbon dioxide from ambient air. *The European Physical Journal Special Topics*, 176(1), pp. 93-106.

Lange, J.-P., 2001. Methanol Synthesis: a short review of technology improvements. *Catalysis Today*, 64(1-2), pp. 3-8.

Lunde, P. J. & Kester, F. L., 1974. Carbon Dioxide Methanation on a Ruthenium Catalyst. *Industrial & Engineering Chemistry Process Design and Development*, 13(1), pp. 27-33.

Martins, J. A., Faria, A. C., Soria, M. A., Miguel, C. V., Alírio, A. E., Madeira, L. M., 2019. CO2 Methanation over Hydrotalcite-Derived Nickel/Ruthenium and Supported Ruthenium Catalysts. *Catalysts,* 9(12), p. 1008.

Mesfun, S., Sanchez, D. L., Leduc, S., Wetterlund, E., Lundgren, J., Biberacher, M., Kraxner, F., 2017. Power-to-gas and power-to-liquid for managing renewable electricity intermittency in the Alpine Region. *Renewable Energy*, Volume 107, pp. 361-372.

Miguel, C. V., Mendes, A. & Madeira, L. M., 2018. Intrinsic kinetics of CO2 methanation over an industrial nickel-based catalyst. *Journal of CO2 Utilization,* Volume 25, pp. 128-136.

Mills, G. A. & Steffgen, F. W., 1974. Catalytic Methanation. *Catalysis Review*, 8(1), pp. 159-210.

National Oceanic and Atmospheric Administration, 2018. [Online] Available at: https://www.ncdc.noaa.gov/paleo-search/study/17975 [Accessed on 08 March 2020].

Palma, V., Meloni, E., Ruocco, C, Martino, M, Ricca, A., 2018. State of the Art of Conventional Reactors for Methanol Production. *Methanol*, Volume 2, pp. 29-51.

Perry, R. & Green, D., 1999. *Perry's Chemical Engineers' Handbook.* 7 ed. New York: McGraw Hill.

Poling, B. E., Prausnitz, J. M. & O'Connel, J. P., 2001. *The Properties of Gases and Liquids.* New York: McGrall-Hill.

Portha, J, Parkhomenko, K., Kobl, K., Roger, A., Arab, S., Commenge, J., Falk, L., 2017. Kinetics of Methanol Synthesis from Carbon Dioxide Hydrogenation over Copper–Zinc Oxide Catalysts. *Industrial & Engineering Chemistry Research*, 56(45), pp. 13133-13145.

Rodrigues, A. E., Madeira, L. M., Wu, Y.-J. & Faria, R., 2017. *Sorption Enhanced Reaction Processes.* s.l.:World Scientific (Sustainable Chemistry Series).

Rokem, J. S. & Greenblat, C. L., 2015. Making Biofuels Competitive: The Limitations of Biology for Fuel Production. *JSM Microbiology,* 3(2), pp. 1-6.

Santangelo, D. L. O., Ahón, V. R. R. & Costa, A. L. H., 2008. Optimization of Methanol Synthesis Loops with Queench Reactors. *Chemical Engineering & Technology*, 31(12), pp. 1767-1774.

Tsao, J., Lewis, N. & Crabtree, G., 2006. *Solar FAQs,* s.l.: US department of Energy.

Veers, P., Dykes, K., Lantz, E., Barth, S., Botasso, C. L., Carlson, O., Clifton, A., Green, J., Green, P., Holttinen, H., Laird, D., Lehtomaki, V., Lundquist, J. K., Manwell, J., Marquis, M., Meneveau, C., Moriarty, P., Munduate, X., Muskulus, M., Naughton, J., Pao, L., Paquette, J., Penke, J., Robertson, A., Rodrigo, J. S., Sempreviva, A. M., Smith, J. C., Tuohy, A., Wiser, R., 2019. Grand challanges in the science of wind energy. *Science,* 366(6464), pp. 1-17.

Vital, J. & Sousa, J. M., 2013. Polymeric membranes for membrane reactors. *Handbook of Membrane Reactors*, Volume 1, pp. 3-41.

Wakao, N. & Funazkri, T., 1978. Effect of fluid dispersion coefficients on particle-to-fluid mass transfer coefficients in packed beds. *Chemical Engineering Science,* 33(10), pp. 1375-1384.

Wang, N., Liu, Y., Huang, A. & Caro, J., 2014. Supported SOD membrane with steam selectivity by a two-step repeated hydrothermal synthesis. *Microporous and Mesoporous Materials*, Volume 192, pp. 8-13.

Wu, Y.-J, Li, P., Yu, J.-G, Cunha, A. F., Rodrigues, A. E., 2016. Progress on sorption-enhanced reaction process for hydrogen production. *Reviews in Chemical Engineering*, 32(3), pp. 1-33.

Appendix A – Physical Properties

The thermodynamic properties for each species considered were the ones represented in Table A-1:

Table A-1 - Thermodynamic properties for the compounds in this work *(Perry & Green, 1999)*.

Property	CO_2	H_2	H_2O	CH_4	CH_3OH	N_2
Molar weight, M_i (g.mol^{-1})	44.01	2.02	18.02	16.04	32.00	28.01
Critical temperature, $T_{c,i}$ (K)	304.2	33.19	647.1	190.7	513.4	126.2
Critical pressure, $P_{c,i}$ (bar)	73.83	13.13	220.55	46.00	82.2	34.00

The dimensionless numbers were defined as (Perry & Green, 1999):

- **Reynolds of the fluid mixture**

$$Re = \frac{\rho_f \, u_0 \, d_p}{\mu_f} \qquad \text{Eq. A-1}$$

Where ρ_f is the density of the fluid mixture, u_0 is the superficial velocity of the fluid mixture, d_p is the diameter of the particle of catalyst and μ_f stands for the viscosity of the fluid mixture.

- **Prandtl of the fluid mixture**

$$Pr = \frac{\mu_f \, C_{p,f}}{\lambda_f} \qquad \text{Eq. A-2}$$

Where $C_{p,f}$ is the molar heat capacity of the fluid mixture at constant pressure and λ_f is the thermal conductivity of the fluid mixture.

- **Schmidt of the fluid mixture**

$$Sc = \frac{\mu_f}{\rho_f \, D_m} \qquad \text{Eq. A-3}$$

Where D_m corresponds to the molecular diffusion of the fluid mixture and was estimated by Eq. A-4 (Rodrigues, *et al.*, 2017):

$$D_m = \sum_{i=1}^{n} D_{m,i} \, y_i \qquad \text{Eq. A-4}$$

Where $D_{m,i}$ is the molecular diffusion of the species i and was determined by Eq. A-5 (Rodrigues, *et al.*, 2017):

$$D_{m,i} = \frac{1 - y_i}{\sum_{j=1}^{n} \frac{y_j}{D_{ij}}} \qquad \text{Eq. A-5}$$

Where D_{ij} stands for the binary diffusivity of the species i is calculated through the Fuller method (Eq. A-6) (Perry & Green, 1999):

$$D_{ij} = \frac{10^{-3}\, T^{1.75} \left(\frac{1}{M_i} + \frac{1}{M_j}\right)}{P \left((\sum v)_i^{1/3} + (\sum v)_j^{1/3} \right)^2} \qquad \text{Eq. A-6}$$

Where $(\sum v)_i$ and $(\sum v)_j$ is the sum of the atomic diffusion volumes for species i and j, respectively. The values considered in this work are presented in Table A-2.

Table A-2 - The sum of the atomic diffusion volumes for each compound *(Perry & Green, 1999)*.

Molecule	Diffusion volume, $\sum v$, $cm^3 \cdot mol^{-1}$
CO_2	26.9
H_2	7.07
H_2O	12.7
CH_4	24.4
CH_3OH	31.25
N_2	17.9

The gas mixture density is given by the Eq. A-7:

$$\rho_f = \frac{P}{R\,T} \sum_{i=1}^{n} (y_i\, M_i) \qquad \text{Eq. A-7}$$

The heat capacity of the fluid mixture is calculated by the Eq. A-8 (Perry & Green, 1999):

$$C_{p,f} = \sum_{i=1}^{n} \frac{y_i\, C_{p,i}}{M_i} \qquad \text{Eq. A-8}$$

Where $C_{p,i}$ is the molar heat capacity of species i, obtained through Eq. A-9 (Perry & Green, 1999):

$$C_{p,i} = A + B\,T + C\,T^2 + D\,T^{-2} \qquad \text{Eq. A-9}$$

Where the coefficients A, B, C, and D for each species are shown in Table A-3.

Table A-3 – Coefficients to estimate the heat capacity of a compound in J·mol^{-1}·K^{-1}.

Species	$\boldsymbol{A}$ (J·mol^{-1}·K^{-1})	$\boldsymbol{B \times 10^3}$ (J·mol^{-1}·K^{-2})	$\boldsymbol{C \times 10^6}$ (J·mol^{-1}·K^{-3})	$\boldsymbol{D \times 10^{-5}}$ (J·mol^{-1}·K)
CO_2	5.457	1.045	0.000	-1.157
H_2	3.249	0.422	0.000	0.083
H_2O	3.470	1.450	0.000	0.121
CH_4	1.702	9.081	-2.164	0.000
CH_3OH	2.221	12.22	-3.450	0.000
N_2	3.280	0.593	0.000	0.040

Therefore, the fluid mixture viscosity is calculated through the Wilke method (Eq. A-10) (Poling, *et al.*, 2001).

$$\mu_f = \sum_{i=1}^{n} \frac{y_i\,\mu_i}{\sum_{j=1}^{n}(y_i\,\phi_{ij})} \qquad \text{Eq. A-10}$$

Where ϕ_{ij}, binary term, is calculated by Eq. A-11 (Davidson, 1993):

$$\phi_{ij} = \frac{\left[1 + \sqrt{\frac{\mu_i}{\mu_j}}\left(\frac{M_j}{M_i}\right)^{1/4}\right]^2}{\left[8\left(1 + \frac{M_j}{M_i}\right)\right]^{1/2}} \qquad \text{Eq. A-11}$$

Where μ_i is the viscosity for the compound i and can be calculated by Eq. A-12 (Perry & Green, 1999):

$$\mu_i = \frac{A\,T^B}{1 + \frac{C}{T} + \frac{D}{T^2}} \qquad \text{Eq. A-12}$$

Where the coefficients A, B, C, and D for each species are presented in Table A-4.

Table A-4 - Coefficients to estimate the viscosity of a compound in Pa·s. Source: Aspen Properties Software

Coefficient	CO_2	H_2	H_2O	CH_4	N_2
A	2.1480 x 10^{-6}	1.7970 x 10^{-7}	1.7096 x 10^{-8}	5.2546 x 10^{-7}	6.5592 x 10^{-7}
B	0.46000	0.68500	1.11460	0.59006	0.60810
C	290.000	-0.590	0.000	105.670	54.714
D	0	140	0	0	0

The thermal conductivity of the fluid mixture is obtained through the Wassijewa method (Eq. A-13) (Poling, *et al.*, 2001):

$$\lambda_f = \sum_{i=1}^{n} \frac{y_i \, \lambda_i}{\sum_{j=1}^{n} (y_j \, A_{ij})} \qquad \text{Eq. A-13}$$

Where λ_i is the thermal conductivity of the compound i and is obtained through Eucken equation (Eq. A-14) (Poling, *et al.*, 2001):

$$\lambda_i = \mu_i \left(1.25 \, \frac{R}{M_i} + \frac{C_{p,i}}{M_i}\right) \qquad \text{Eq. A-14}$$

Where A_{ij} is the binary interaction parameter based on Mason and Saxena (Eq. A-15) (Poling, *et al.*, 2001):

$$A_{ij} = \frac{\left[1 + \left(\frac{\lambda_{tr,i}}{\lambda_{tr,j}}\right)^{1/2} + \left(\frac{M_i}{M_j}\right)^{1/4}\right]^2}{\left[8\left(1 + \frac{M_i}{M_j}\right)\right]^{0.5}} \qquad \text{Eq. A-15}$$

Where $\frac{\lambda_{tr,i}}{\lambda_{tr,j}}$ corresponds to the translational thermal conductivities and can be obtained from Eq. A-16 (Poling, *et al.*, 2001):

$$\frac{\lambda_{tr,i}}{\lambda_{tr,j}} = \frac{\Gamma_j \left[exp\left(0.0464 \, T_{r,i}\right) - exp\left(-0.2412 \, T_{r,i}\right)\right]}{\Gamma_i \left[exp\left(0.0464 \, T_{r,j}\right) - exp\left(-0.2412 \, T_{r,j}\right)\right]} \qquad \text{Eq. A-16}$$

Where $T_{r,i}$ is the reduced temperature of species i and is equal to $T/T_{c,i}$. Therefore, Γ_i (m·K·W^{-1}) is obtained from Eq. A-17 (Perry & Green, 1999):

$$\Gamma_i = 210 \left(\frac{T_{c,i} \, {M_i}^3}{{P_{c,i}}^4} \right)^{1/6} \qquad \text{Eq. A-17}$$

The mass axial dispersion is obtained through the Equation A-18:

$$D_{ea} = \frac{u_0 \, d_p}{\varepsilon_b \, Pe} \qquad \text{Eq. A-18}$$

Where Pe is the Peclet number and it is a function of Reynolds Number (Re) and Schmidt Number (Sc) and is represented by Eq. A-19 (Perry & Green, 1999):

$$\frac{1}{Pe} = \frac{0.3 \, \varepsilon_b}{Re \, Sc} + \frac{0.5}{1 + \frac{3.8}{Re \, Sc}} \qquad \text{Eq. A-19}$$

Finally, the axial heat dispersion coefficient is obtained through the Wakao and Funazkri correlation Eq. A-20 (Wakao & Funazkri, 1978):

$$\lambda_{ae} = 7 \, \lambda_f + 0.5 \, \rho_f \, u_0 \, d_p \, C_{p,f} \qquad \text{Eq. A-20}$$

Appendix B – Global Coefficient of Heat Transfer

For the traditional reactor, the global coefficient of heat transfer, U^R, is obtained by Equation B-1:

$$\frac{1}{U^R} = \frac{1}{h^R} + \frac{A^R \; ln\left[\left(r^R + \delta^{shell}\right)/r^R\right]}{2\,\pi\,L\,k^{shell}} + \frac{A^R}{A^{shell}}\;\frac{1}{h^{out}} \qquad \text{Eq. B-1}$$

Where δ^{shell} is the shell thickness; k^{shell} is the shell thermal conductivity (equal to 14.4 $W \cdot m^{-1} \cdot K^{-1}$, for stainless steel) and h^{out} is the convective heat transfer coefficient in the oven (equal to 50 $W \cdot m^{-2} \cdot K^{-1}$, as natural convection of air). (Perry & Green, 1999).

For the membrane reactor, the global coefficient of heat transfer from the retentate to the permeate side, U^R, is determined through Equation B-2:

$$\frac{1}{U^R} = \frac{1}{h^R} + \frac{A^R \; ln[(r^R + \delta^m)/r^R]}{2\,\pi\,L\,k^m} \qquad \text{Eq. B-2}$$

Where δ^m is the membrane thickness and k^m is the membrane conductivity (equal to 1.2 $W \cdot m^{-1} \cdot K^{-1}$, for a silica MFI-type zeolite).

Moreover, the heat transfer coefficient between the gaseous phase and the membrane, h^R, is calculated by Eq. from Li-Finlayson:

$$h^R = 0.17\,\frac{\lambda_f}{d_p}\,\left(\frac{Pr}{0.7}\right)^{1/3}\,Re^{0.79} \qquad \text{Eq. B-3}$$

Where λ_f is the fluid mixture conductivity, d_p the catalyst particle diameter, Re, and Pr are the Reynolds and Prandtl dimensionless numbers.

The global coefficient for heat flux, U^P, from the permeate side to the exterior is estimated by Equation B-4:

$$\frac{1}{U^P} = \frac{1}{h^P} + \frac{{A_L}^P \; ln[r^{shell}/r^P]}{2\,\pi\,L\,k^{shell}} + \frac{{A_L}^P}{{A_L}^{shell}}\;\frac{1}{h^{out}} \qquad \text{Eq. B-4}$$

Moreover, the coefficient h^P was estimated considering internal forced convection in non-circular tubes according to the following equations (Perry & Green, 1999):

$$h^P = \frac{{\lambda_f}^P}{D_h}\,(Nu)_{annular} \qquad \text{Eq. B-5}$$

$$(Nu)_{annular} = 0.86\,(Nu)_{cylinder}\left(\frac{r^P}{r^R + \delta^m}\right)^{0.16}$$ Eq. B-6

$$(Nu)_{cylinder} = 3.66 + \frac{0.0668\left(\frac{2\,r^P}{L}\right) Re\,Pr}{1 + 0.04\left[\left(\frac{2\,r^P}{L}\right) Re\,Pr\right]^{2/3}}$$ Eq. B-7

In which λ_f^P is the gas thermal conductivity in the permeate side, D_h is the hydraulic diameter, $(Nu)_{annular}$ is the Nusselt dimensionless number described for flow in noncircular ducts and $(Nu)_{cylinder}$ is the Nusselt dimensionless number for flow in round cylinders.